Molecular Pharmacology Fast Forward. Published on December 14, 2009 as doi: 10.1124/mol.109.061366
This article has not been copyedited and formatted. The final version may differ from this version.

MOL #61366

Pleiotropic Effects of YC-1 Selectively Inhibits Pathological Retinal Neovascularization and Promotes Physiological Revascularization in a Mouse Model of Oxygen-Induced Retinopathy

M. DeNiro; A. Al-Halafi; FH. Al-Mohanna; O. Alsmadi; and FA. Al-Mohanna

Research Department, King Khaled Eye Specialist Hospital, Riyadh, Saudi Arabia; (**MD**)

Department of Comparative Medicine, Research Center, King Faisal Specialist Hospital & Research Centre, Riyadh, Saudi Arabia; (**MD, and FHA**)

University of California, San Diego / Shiley Eye Center, La Jolla, CA, USA; (**AA**)

Vitreoretinal Division, King Khaled Eye Specialist Hospital, Riyadh, Saudi Arabia; (**AA**)

Department of Genetics, Research Center, King Faisal Specialist Hospital & Research Center, Riyadh, Saudi Arabia; (**OA**)

Department of Biological and Medical Research, King Faisal Specialist Hospital and Research Centre, Riyadh, Saudi Arabia; (**FAA**)

Molecular Pharmacology Fast Forward. Published on December 14, 2009 as DOI: 10.1124/mol.109.061366
This article has not been copyedited and formatted. The final version may differ from this version.

A. Running Title: Suppression of Pathologic Retinal Neovascularization by YC-1

B. Citations: The article will be cited as: **M. DeNiro *et al*.**

C. Correspondence: Michael DeNiro, King Khaled Eye Specialist Hospital, Aruba Street, P.O. Box.7191, Riyadh 11462, Kingdom of Saudi Arabia

E-mail: mdeniro@kkesh.med.sa

Telephone: (966) 55 787 5950

D. Number of Text Pages: 60

Number of Tables: 0

Number of Figures: 11

Number of Supplementary Figures: 2

Number of References: 95

Number of Words in the Abstract: 250

Number of Words in the Introduction: 1804

Number of Words in the Discussion: 2060

E. Nonstandard Abbreviations

HIF-1	Hypoxia-Inducible Factor-1
iNOS	Inducible Nitric Oxide Synthase
NV	Neovascularization
OIR	Oxygen-Induced Retinopathy
RV	Revascularization
YC-1	3-(5'-hydroxymethyl-2'furyl)-1-benzyl indazole

Molecular Pharmacology Fast Forward. Published on December 14, 2009 as DOI: 10.1124/mol.109.061366
This article has not been copyedited and formatted. The final version may differ from this version.

ABSTRACT

VEGF and iNOS have been implicated in ischemia-induced retinal neovascularization. Retinal ischemia has been shown to induce VEGF and iNOS expression. It has been postulated that one of the crucial consequences of iNOS expression in the ischemic retina, is the inhibition of angiogenesis. Furthermore, iNOS was shown to be over-expressed in Müller cells from patients with diabetic retinopathy. YC-1, a small molecule inhibitor of HIF-1α, has been shown to inhibit iNOS expression in various tissue models. Our aim was to assess the pleiotropic effects of YC-1 in an OIR mouse model, and evaluate its therapeutic potential in HIF-1- and iNOS-mediated retinal pathologies. Dual-injections of YC-1 into the neovascular retinas decreased the total retinopathy score, inhibited vaso-obliteration and pathologic tuft formation, while concomitantly promoting physiological retinal revascularization, when compared with DMSO-treated group. Furthermore, YC-1-treated retinas exhibited a marked increase in immunoreactivities for CD31 and vWF, and displayed significant inhibition in HIF-1α protein expression. Furthermore, YC-1 down-regulated VEGF, EPO, ET-1, MMP-9, and iNOS message and protein levels. When hypoxic Müller and neuoroglial cells treated with YC-1, iNOS mRNA and protein levels were reduced in a dose-dependent fashion. We demonstrate that YC-1 inhibits pathological retinal neovascularization by exhibiting anti-neovascular activities, which impaired ischemia-induced expression of HIF-1 and its downstream angiogenic molecules. Furthermore, YC-1 enhanced physiological revascularization of the retinal vascular plexuses via the inhibition of iNOS mRNA and protein expressions. The pleiotropic effects of YC-1 allude to its possible use as a promising therapeutic iNOS inhibitor candidate for the treatment of retinal neovascularization.

Molecular Pharmacology Fast Forward. Published on December 14, 2009 as DOI: 10.1124/mol.109.061366
This article has not been copyedited and formatted. The final version may differ from this version.

INTRODUCTION

Retinal neovascularization (NV) is the major cause of severe vision loss and irreversible blindness in developed countries, affecting people of all ages (Lee and Adamis, 1998). These clinical and pathologic manifestations occur in diabetic retinopathy, retinopathy of prematurity (ROP), age-related macular degeneration (ARMD) and retinal vein occlusion (RVO). The early stages of retinopathy result from retinal ischemia due to non-perfusion of the retina or a decrease in oxygen tension (Barinaga, 1995). In the late stages, the ischemia-induced pathologic growth of new blood vessels can cause catastrophic loss of vision.

Hypoxia-inducible factor-1 (HIF-1) is a heterodimer that play important roles in embryonic vascularization, angiogenesis, and apoptosis. Under hypoxic/ischemic conditions, and due to the inhibition of proline hydroxylase/VHL degradation pathway (Semenza, 2000), and the consequent stabilization of the α subunit, HIF-1 binds to the hypoxia response element in hypoxia-responsive target genes, and triggers the transcription of many genes such as Vascular Endothelial Growth Factor (VEGF) (Pe'er *et al*., 1995; Forsythe *et al*., 1996), Inducible Nitric Oxide Synthase (iNOS) (Melillo *et al*., 1995), Erythropoietin (EPO) (Wang and Semenza, 1996), and Endothelin-1 (ET-1) (Hu *et al*., 1998).

Oxygen-induced retinopathy (OIR) is a model for human retinopathy of prematurity (ROP). The mouse model for OIR was introduced by Smith *et al*., 1994, and it is widely used to study retinal neovascularization *in vivo*. In this model, P7 mice were exposed for 5 days (P7-P12) to hyperoxic conditions (75% O_2) producing vaso-obliteration (over 60% of the retinal vasculature is lost during this stage), and cessation of vascular development in the capillary beds of the central retina. In addition, exposure to hyperoxia induces vessel regression via selective apoptosis of vascular endothelial cells (Yamada *et al*., 1999; Alon *et al*., 1995). On P12, mice are

Molecular Pharmacology Fast Forward. Published on December 14, 2009 as DOI: 10.1124/mol.109.061366
This article has not been copyedited and formatted. The final version may differ from this version.

returned to room air, i.e., normoxia; relative hypoxia ensues in the severely hypovascular central retina, causing abnormal vascular growth. As a result, HIF-1 is over-expressed, VEGF is up-regulated, and pathological conditions will lead to angio-proliferation in the immature retina over the next 3-5 days (P17). These retinal pathologies will ultimately cause the development of retinal neovascularization (Pierce *et al*., 1995; Ozaki *et al*., 2000). Around P15 the retinal ischemia initiates an aggressive neovascular response at the interface of the perfused retinal periphery and the ischemic central capillary beds. In addition, VEGF is up-regulated and preretinal neovascularization appears between P15 and P21 with maximal neovascularization at P17 (Pierce *et al*., 1995; Ozaki *et al*., 2000).

Clinical and experimental observations have indicated that ischemia triggers retinal NV through an excessive production of one or more angiogenic factors. Furthermore, pathologic angiogenesis in the mouse model of OIR is known to be regulated by ischemia-mediated expression of angiogenic factors such as VEGF (Ishida *et al*., 2003). When cells incubated under hypoxic conditions, oxygen becomes limiting, and HIF-1α accumulates within the cells, and ultimately several downstream molecules, such as VEGF, EPO, and iNOS are up-regulated. VEGF has a profound impact on multiple functions in endothelial cells, such as proliferation, migration, survival, tube formation, and vascular permeability (Cross *et al*., 2003; Matsumoto *et al*., 2001). In addition, previous data have indicated that increased levels of HIF-1α in ischemic retinas correlated temporally and spatially with the increased expression of VEGF in such a way that HIF-1α preceded the up-regulation of VEGF (Ozaki *et al*., 1999). Furthermore, retinal ischemia is the major driving force behind the induction of VEGF, which plays a crucial role in ocular pathogenesis (Campochiaro, 2000). Several studies have indicated that no single growth factor acts alone to cause retinal NV. Such interaction occurs between basic fibroblast growth

factor (bFGF) and VEGF in the induction of angiogenesis. There is substantial evidence to indicate that EPO, which is a potent ischemia-induced angiogenic factor, acts independently of VEGF during retinal angiogenesis in proliferative diabetic retinopathy (PDR) (Watanabe *et al*., 2005; Jaquet *et al*., 2002). Another pro-angiogenic factor that has been implicated in pre-retinal NV, including diabetic retinopathy and ROP, is Matrix Metalloproteinase-9 (MMP-9). Studies by Das *et al*. (1999) indicated that both MMP-2 and MMP-9 are present in neovascular diabetic membranes and that MMP-2 and -9 retinal mRNAs and proteins are increased in mice with ischemia-induced retinal NV (Das *et al*., 1999). In addition, MMP-9 plays a major role in the pathogenesis of diabetic retinopathy, and in choroidal neovascularization (CNV) (Steen *et al*., 1998; Das *et al*., 1999; Majka *et al*., 2001; Zhang *et al*., 2002; Sivak *et al*., 2002; Lambert *et al*., 2002; Lambert *et al*., 2003). Moreover, Endothelin-1 (ET-1) is another pro-angiogenic factor, which is produced by endothelial cells (Inoue *et al*., 1999) and induced by HIF-1-signaling (Hu *et al*., 1998). ET-1 exhibits a substantial increase in the mRNA levels in the retinas of chronic diabetic BB/W rats (Chakrabarti and Sima, 1997). Additionally, ET-1 is involved in various stages of neovascularization from endothelial cell proliferation to stimulation of endothelial cell migration, invasion, protease production, and tube formation (Salani *et al*., 2000). Furthermore, ET-1 secretion has been implicated in retinal hyperoxic vasoconstriction (Takagi *et al*., 1996), and it has been shown that hyperoxia stimulates ET-1 secretion from endothelial cells (Higgins *et al*., 1998). Moreover, ET-1 expression in the retina increased 4.1-fold from P7 to P12 and a 1.9-fold increase from P12 to P17. Overall, there was an 8-fold increase in ET-1 expression from P7 to P17 (Tadesse *et al*., 2001).

Nitric oxide (NO) is a crucial signaling molecule that mediates a variety of essential processes, including neurotransmission, and vasodilatation (Christopherson and Bredt, 1997).

Molecular Pharmacology Fast Forward. Published on December 14, 2009 as DOI: 10.1124/mol.109.061366
This article has not been copyedited and formatted. The final version may differ from this version.

Furthermore, NO has also been implicated in the pathogenesis of retinal injury from hypoxia/ischemia (Adachi *et al*., 1998), and it has been shown to exert negative effects in diabetic retinopathy, glaucoma, and ROP. Data have indicated that cytokine- and growth factor-inducible NO synthase (iNOS) is associated with production of large quantities of NO (Chiou *et al*., 2001). Moreover, NO is known to influence neovascularization in a variety of models of angiogenesis, and its effect can be pro-angiogenic (Parenti *et al*., 1998; Ziche *et al*., 1997; Papapetropoulos *et al*., 1997) or anti-angiogenic (Tsurumi *et al*., 1997; Liu *et al*., 1998; Tuder *et al*., 1995). These seemingly contradictory data may be explained by the action of different nitric oxide synthase (NOS) isoforms in the different models used. The role of nNOS in angiogenesis remains undetermined (Borda *et al*., 2005); however, there is increasing evidence that endothelial NOS (eNOS) play a pro-angiogenic role (Fulton *et al*., 1999; Murohara *et al*., 1998). Previous studies have indicated that the effects of inducible NO synthase (iNOS) were contradictory with both (Sennlaub *et al*., 1999; Pipili-Synetos *et al*., 2000), and pro-angiogenic (He *et al*., 2007; Hattenbach *et al*., 2002). The current manuscript focused on the effect of YC-1 on iNOS inhibition, and ultimately the impact of YC-1 on retinal NV. Sennlaub *et al*. (2001) and Kobayashi *et al*. (2000) have both shown that iNOS is induced in ischemic proliferative retinopathy. In addition, iNOS induction by hypoxia has been demonstrated by others *in vitro* (Melillo *et al*. 1995) and *in vivo* (Palmer *et al*., 1998). Hypoxia inducible factor-1 (HIF-1) is up-regulated in the murine model of ischemic proliferative retinopathy (Ozaki *et al*., 1999). Because the consensus sequence for HIF-1 transcription factor is present in the promoter of iNOS (Melillo, *et al*. 1995), HIF could be responsible for iNOS induction in the ischemic retina. In recent years, accumulating evidence suggests that inflammation is a key event in the pathogenesis of diabetic vascular complications (Abu El-Asrar *et al*. 1997; Mitamura *et al*. 2001;

Molecular Pharmacology Fast Forward. Published on December 14, 2009 as DOI: 10.1124/mol.109.061366
This article has not been copyedited and formatted. The final version may differ from this version.

Hernández *et al*. 2005). During diabetic retinopathy, the expression of iNOS is up-regulated and is thought to play a key role in the pathogenesis of retinal neovascularization. Nitric oxide (NO), derived from iNOS, regulates the expression of P-selectin and ICAM-1 and contributes to vasodilatation (Lush *et al*., 2001; Cuzzocrea *et al*., 2002; Hierholzer *et al*., 2004). In addition, iNOS expression in the retina is likely to cause tissue damage by interfering with the beneficial activities of constitutive neuronal NOS and endothelial NOS (Thillaye-Goldenberg *et al*., 2000; Liversidge *et al*., 2002; Rajendram *et al*., 2007). Previous data have indicated that YC-1 profoundly blocked LPS-induced up-regulation of iNOS expression in tissues of the endotoxemic mouse model (Pan *et al*., 2005). In addition, previous investigations have confirmed the up-regulation of both VEGF and iNOS in the retina of OIR models. The up-regulations of both VEGF and iNOS indicate their pathological roles in the retinal NV (Kaur *et al*., 2006). Moreover, it has been revealed that VEGF induce the expression of iNOS **(**Kroll *et al*., 1998) and stimulate production of NO (Van der Zee *et al*., 1997). Müller cells, which are astrocyte-like radial glial cells that extend vertically throughout the retina, are thought to play an important role in pathologic processes of retinal wound healing and NV. Additionally, they control the onset of endothelial activation and neovascularization largely by releasing anti-angiogenic cytokines. Moreover, massive local proliferation of Müller cells is a key feature of retinal proliferative disorders. Data have identified iNOS as one of the major contributors to NO production in Müller cells (Du and Kern, 2004), and several investigations have demonstrated that rat Müller cells (rMC–1) can be used as an *in vitro* model to study the VEGF induction pathway in ischemia–induced retinal angiogenesis (Qi *et al*., 2004). Moreover, iNOS immunoreactivity was up-regulated in retinal Müller glial cells from human patients with nonproliferative diabetic retinopathy (Abu El-Asrar *et al*., 2004).

YC-1 is a small molecule HIF-1 inhibitor, which potentiates soluble guanylyl cyclase (sGC) stimulation. In a previously published chemical structure of YC-1; [3-(5'-hydroxymethyl-2'furyl)-1-benzyl indazole], Ko *et al*., (1994) have indicated that the synthetic chemical benzylindazole compound, YC-1, possessed antiplatelet activity and potentiated soluble guanylyl cyclase (sGC) stimulation. In platelets and vascular smooth muscle, the administration of YC-1 is accompanied by an increase in the intracellular cGMP concentration, which occurs via the stimulation of soluble guanylate cyclase (sGC) (Teng *et al*., 1997; Galle *et al*., 1999). We have recently demonstrated that YC-1 down-regulates HIF-1α, HIF-2α, VEGF, EPO, ET-1, and MMP-9 protein levels in the human retinal microvascular endothelial cells (DeNiro *et al*., 2009). During this study we hypothesized the followings; (1) YC-1 possesses novel pleiotropic effects, which could impair ischemia-induced expression of HIF-1 and its downstream angiogenic molecules. This may ultimately inhibit retinal neovascularization progression by exhibiting novel anti-angiogenic properties via impeding HIF-1- and iNOS-mediated retinal pathologies; (2) YC-1 may selectively inhibit pathological NV while concomitantly promotes physiological RV in a mouse model of ischemic retinopathy; (3) In addition to being a potent HIF-1 inhibitor and due to its pleiotropic effects, YC-1 could play a major role in the inhibition of iNOS expression in the retina and may ultimately become a potential candidate for the treatment of retinal neovascularization. This manuscript reveals that YC-1 selectively inhibits pathological NV while concomitantly promotes physiological RV in a mouse model of OIR. The current study investigates the efficacy of YC-1 in modulating iNOS expression as a therapeutic modality to target retinal NV *in vivo,* and examines the therapeutic potentials of utilizing YC-1 as a HIF-1 and an iNOS inhibitor.

Molecular Pharmacology Fast Forward. Published on December 14, 2009 as DOI: 10.1124/mol.109.061366
This article has not been copyedited and formatted. The final version may differ from this version.

MATERIALS and METHODS

Reagents

YC-1; [3-(5'-hydroxymethyl-2'furyl)-1-benzyl indazole], (Ko *et al*., 1994).
was purchased from A.G. Scientific (San Diego, CA) and dissolved in sterile dimethyl sulfoxide (DMSO). Fluorescein isothiocyanate (FITC)-dextran 2,000,000 was purchased from Sigma-Aldrich (St. Louis, MO). Monoclonal mouse anti-HIF-1α (clone H1α67) and monoclonal rabbit anti-VEGF antibodies were both purchased from Millipore (Billerica, MA). Polyclonal goat anti-Erythropoietin (EPO) antibody was purchased from Santa Cruz Biotechnology (Santa Cruz, CA). Polyclonal rabbit anti-Endothelin-1 (ET-1) antibody was purchased from Abbiotec (San Diego, CA). Monoclonal mouse anti-MMP-9 antibody was purchased from Neuromab (Davis, CA). For iNOS *Western blot* and *Immunofluorescence staining*; monoclonal mouse anti-iNOS antibody was purchased from Abcam (Cambridge, MA); whereas, monoclonal mouse anti-iNOS antibody, which was purchased from BD Biosciences (San Diego, CA), was used in all *immunohistochemistry staining*. Monoclonal rat anti-mouse platelet endothelial cell adhesion molecule-1 (PECAM-1, also known as CD31) antibody was purchased from BD Biosciences (Franklin Lakes, NJ). Polyclonal rabbit anti-von Willebrand Factor (vWF) antibody was purchased from Abcam (Cambridge, MA). Polyclonal rabbit anti-β-actin antibody was purchased from MBL Intl (Woburn, MA).

Animals and Experimental Design

C57BL/6J mice, from Jackson Laboratory (Bar harbor, ME) were used in these experiments. All animal protocols were approved by the Institutional Review Board and conformed to the ARVO Statement for the Use of Animals in Ophthalmic and Vision Research statement of the

Molecular Pharmacology Fast Forward. Published on December 14, 2009 as DOI: 10.1124/mol.109.061366
This article has not been copyedited and formatted. The final version may differ from this version.

Association for Research in Vision and Ophthalmology. Mice were divided into four separate groups; (1) Non-treated mice grown under ambient conditions (negative control); (2) non-treated hyperoxia-exposed mice (positive control); (3) DMSO- treated hyperoxia-exposed mice (sham-treated); and (4) YC-1-treated hyperoxia-exposed mice (drug-treated).

Mouse Model of Oxygen Induced Retinopathy

As outlined in Fig. 1, retinal NV was induced in newborn mice as described previously (Smith *et al*., 1994). Briefly, P7 mice were exposed with their nursing mother, for 5 days (between P7 and P12) to hyperoxic conditions, by incubating them in an airtight chamber (PROOX 110 chamber O_2 controller; Biospherix Ltd., Redfield, NY) ventilated by a mixture of O_2 and air to a final oxygen fraction of 75 ± 2%. These incubation conditions induced vaso-obliteration and subsequent cessation of vascular development in the capillary beds of the central retina (Smith *et al*., 1994). At P12, the mice were allowed to recover in normal room air conditions and maintained for another 5 days (till P17), the day in which peak disease occurs. A condition of relative hypoxia resulted between P12 and P17, and extensive retinal NV developed in 100% of the mice. Age-matched animals with the hyperoxia-exposed groups were maintained identically, except they were exposed to room air (21% O2, 79% N2) for the entire duration of the experiment. All animals were examined and sacrificed on the same days.

Intravitreal Injections

A group of hyperoxia-exposed animals (n=15) were injected intravitreally (into both eyes), immediately after removal from 5-day treatment of 75% oxygen, at P12 and P15 with 3 μl of YC-1 (100 μM) [drug-treated group]. Another group of hyperoxia-exposed mice (n=15) were

Molecular Pharmacology Fast Forward. Published on December 14, 2009 as DOI: 10.1124/mol.109.061366
This article has not been copyedited and formatted. The final version may differ from this version.

injected intravitreally (into both eyes), immediately after removal from 5-day treatment of 75% oxygen, at P12 and P15 with 3 μl of DMSO (0.2% [v/v]) [sham-treated group]. Non-treated mice grown under ambient conditions, non-treated hyperoxia-exposed mice, DMSO- treated hyperoxia-exposed mice and YC-1-treated hyperoxia-exposed mice, were all examined at different critical time points for qualitative assessment of the retinal vasculature by fluorescein angiography.

Retinal Fluorescein Angiography with High-Molecular-Weight Fluorescein-Dextran

Mice were anesthetized with an intraperitoneal injection of a ketamine (100 mg/kg) and xylazine (15 mg/kg) solution. Mice were then perfused through the left ventricle with 600 μL of high-molecular-mass (2 X 10^6 Da) FITC-dextran in PBS (50 mg/ml), which was allowed to circulate for 2 minutes before the animals were euthanatized and the eyes enucleated. Subsequent to retinal extraction, all retinas were fixed in 4% paraformaldehye for 24 hrs at 4°C. A dissecting microscope was used to remove the cornea and lens and gently separate the retina from the underlying choroid and sclera. Microscissors were used to make four radial incisions of the retinal eyecup in order to prepare retinal flat mounts on glass slides. Flat mounts were immersed in Aquamount mounting medium (Polysciences, Warrington, PA), coverslips were carefully placed over the retina, and the edges of the coverslips were sealed.

Histological Analysis of Retinal Sections and Quantification of Extra-retinal NV

Mice were sacrificed using sodium pentobarbital. After midline sternotomy was performed, the left ventricle was injected with 4% paraformaldehyde in PBS. The eyes were enucleated, placed immediately in optimum cutting temperature embedding compound (Sakura Fine Tek, Torrence,

Molecular Pharmacology Fast Forward. Published on December 14, 2009 as DOI: 10.1124/mol.109.061366
This article has not been copyedited and formatted. The final version may differ from this version.

CA), and frozen at -70°C. Serial 5-µm-thick sections of the eye were cut and stained with Hematoxylin and Eosin (H&E). Sections from individual retinas were scored in a masked fashion using light microscopy (Zeiss Axiovert 135, Thornwood, NY). Digital images of representative sites were acquired at X63 or X200 magnification (AxioCam, NY). All nuclei extending beyond the ILM into the vitreous were counted as previously described (Smith *et al*., 1994). Efficacy of treatment was calculated as the percentage of average of nuclei per section in the eyes of YC-1-treated mice versus non-treated ischemic retina. A minimum of 10 sections at least 50 µm apart were evaluated and counted per eye and then averaged. The average neovascular nuclei ± SEM per section per eye was used in the statistical analysis.

Quantification of Retinal Vasculature and Scoring of Retinal NV

Retinopathy score of retinal whole mounts was performed using fluorescent microscopy (Zeiss Axiovert 135, Thornwood, NY), and images were acquired using a 10X and 100X objectives using a digital camera (AxioCam, NY). The extent of retinal NV was then by conducting a combination of; (1) retinal fluorescein angiography; (2) fluorescent microscopy, to analyze the retinopathy score; (3) Metamorph™ imaging software (Universal Imaging, Sunnyvale, CA), to quantify the extent of retinal NV; and ultimately, (4) Implementing the retinal NV scoring system as previously described (Higgins *et al*., 1999). Briefly, the entire retina was outlined to distinguish the total retinal area of each eye. Then, the images were thresholded to emphasize only the FITC-perfused vessels. This permitted the measurement of total blood vessel area of each retina and the percentage of each retina that is engrossed with blood vessels. Furthermore, Retinal NV scoring was performed as previously described (Higgins *et al*., 1999). Briefly, the retinopathy scoring system was developed using a modification of a previously described scoring

Molecular Pharmacology Fast Forward. Published on December 14, 2009 as DOI: 10.1124/mol.109.061366
This article has not been copyedited and formatted. The final version may differ from this version.

system for the kitten (Phelps *et al*., 1977; Phelps *et al*., 1984; Higgins *et al*., 1990) and the ICROP (Anonymous. 1984) that is used clinically in the neonatal intensive care unit. The scoring system is shown in Fig. 4B. Blood vessel growth and central vasoconstriction (loss of central vasculature) delineate the degree of immaturity seen postnatally in the mouse and the degree of injury caused by the hyperoxia. Vasoconstriction or loss of central vessels is manifested in human ROP as vasoconstriction and vaso-obliteration in the growing vessel front followed by the development of a retinopathy in the preterm infant. Neonatal retinal vasoconstriction has been shown to occur at arterial oxygen tensions above 100 mm Hg (Aranda *et al*., 1971). The healing or vaso-proliferative phase was scored based on; (1) the size of the central avascular area; (2) blood vessel tuft formation; (2) extra retinal neovascularization; and (4) presence of blood vessel tortuosity. Degree of maturity (*i.e.* distance of growth of the blood vessels from the center of the retina to the periphery) is defined by arbitrarily dividing the retina into three zones similar to the ICROP method (Anonymous. 1984). For the purposes of this model, we divided the retina into three areas: zone 1 or the inner circumferential third of the retina around the optic disc, zone 2, or the middle third of the retina; and zone 3, or the outer third of the retina. The extent of disease was specified by clock hours or distance around the retina (number of twelfths similar to a clock) in the same fashion as the ICROP method (Anonymous. 1984). The scoring was performed in a masked fashion, by employing fluorescence microscopy (Zeiss Axiovision, Thorwood, NY), evaluating and scoring each retina in a blinded manner by three observers. The minimum score according to this method is 0, and the maximum score is 13. Maximal vaso-proliferation in this mouse model has previously been reported to occur from P17 to P21 (Smith *et al*., 1994). The average retinopathy score for each animal was used for statistical analysis.

Molecular Pharmacology Fast Forward. Published on December 14, 2009 as DOI: 10.1124/mol.109.061366
This article has not been copyedited and formatted. The final version may differ from this version.

Quantitative Assessment of Vascular Density in the Retinal Microvasculature

Retinas were harvested at various time points and fixed with 4% paraformaldehyde (PFA) and methanol followed by blocking in 50% FBS/20% normal goat serum for 1 hour at room temperature. To stain retinal vasculature, retinas were incubated with anti-CD31 or anti-vWF antibodies. The sections were washed with TBST and incubated with EnVision Polymer HRP secondary antibody (DAKO, Carpinteria, CA) for 30 minutes. Light microscopy (Zeiss Axiovert 135, Thornwood, NY) was employed and images were acquired using a digital camera (AxioCam, NY) at X63 objectives.

Quantitative RT-PCR by Molecular Beacon Assays

mRNA levels for all genes (*HIF-1α, VEGF, EPO, ET-1, MMP-9*, and *iNOS)* were quantified by Real time RT-PCR. We used the primers summarized in (Fig. 8G) for RT-PCR. Gene-specific molecular beacons and primers were designed to encompass the genes of interest, with beacon's annealing site to overlap with the exon-exon junctions for additional specificity [(Beacon Designer 6.0, Premier Biosoft International, Palo Alto, CA, USA) (Fig. 8G). Threshold cycle (Ct) values for the different samples were utilized for the calculation of gene expression fold change using the formula 2 to the minus power of delta delta ct. Fold changes in the (*HIF-1α, VEGF, EPO, ET-1, MMP-9*, and *iNOS*) gene relative to the *β-actin* endogenous control gene were determined by the following equation: fold change = $2^{-\Delta\ (\Delta C_T)}$, where change in threshold cycle (ΔC_T) = C_T (*gene of interest*) – C_T (*β-actin*) and Δ (ΔC_T) = ΔC_T (treated) – ΔC_T (untreated).

Molecular Pharmacology Fast Forward. Published on December 14, 2009 as DOI: 10.1124/mol.109.061366
This article has not been copyedited and formatted. The final version may differ from this version.

Retinal Immunohistochemistry

Mouse retinas were dissected and prepared for immunohistochemical analysis, fixed in 4% paraformaldehyde in 0.1 M PBS for 15 min at room temperature and embedded in paraffin, sectioned (5 μm). Tissue sections were deparaffinized, hydrated, and later exposed to heat-induced antigen retrieval using a microwave oven (three 5-minute cycles in citrate buffer, pH 6.0), endogenous peroxidase was abolished with methanol, and hydrogen peroxide and nonspecific background staining was blocked by incubating the tissue sections for 5 minutes in normal swine serum. Subsequently, all slides were washed three times in PBS, and incubated for 1 hour with primary anti–[HIF-1α, VEGF, EPO, ET-1, MMP-9, iNOS, and β-actin] antibodies. The sections were washed with TBST and incubated with EnVision Polymer HRP secondary antibody (DAKO, Carpinteria, CA) for 30 minutes. All slides were stained with DAB solution and counterstained with hematoxylin. Slides were cover slipped (Permount; Fisher Scientific, Fairlawn, NJ) and examined by light microscopy. Negative controls were performed by omitting the primary antibodies. Sections were photographed under a microscope (Zeiss Axiovert 135, Thornwood, NY), and images were acquired a digital camera (AxioCam, NY). All retinas were examined at X60 objective. The staining intensity in our series ranged from a weak blush to moderate or strong. The amount of cells staining with the antibody was further categorized as focal (<10%), patchy (10%-50%), and diffuse (>50%). Equivocal staining was defined as focal and/or weak staining, whereas patchy or diffuse staining was subcategorized as either moderate or strong. All Immunohistochemical analyses were measured by Metamorph digital image analysis software (Molecular Devices, Sunnyvale, CA).

Molecular Pharmacology Fast Forward. Published on December 14, 2009 as DOI: 10.1124/mol.109.061366
This article has not been copyedited and formatted. The final version may differ from this version.

Quantitative Image Analysis of Retinal and Cellular Immunohistochemical Staining

After IHC staining, micrographs were analyzed with Metamorph 7.1 image analysis software (Universal Imaging; Downingtown, PA). This software was used to identify and quantitate the HIF-1α-, VEGF-, EPO-, ET-1-, MMP-9-, and iNOS- immunopositive-stained retinal cells, as described previously in (Nishijima et al., 2007). Briefly, each retinal section was scanned and 30 to 45 one mm^2 regions were chosen from each retinal section for analysis. Color thresholding was used to distinguish the brown DAB signal representing positive immunoreactivity. Images were processed using ImageJ (National Institutes of Health, Bethesda, MD) and Metamorph 7.1 image analysis software (Universal Imaging; Downingtown, PA). To assess background readings, we have quantified all of the above proteins in the retinal sections of non-treated normoxic retinas. The background of images was subtracted, and they were converted to grayscale and binarized using a threshold value derived by: threshold = (average intensity of image + 1 SD of the intensity of image). Background noise and debris were removed using a one-step erosion procedure, and then all remaining objects were counted. The number of immunopositive-stained cells per image was expressed per um^2, and the average number per retinal flat mount was determined among five separate fields.

Assessments of the Retinal Immunohistochemical Analyses for HIF-1α, VEGF, EPO, ET-1, MMP-9, and iNOS Expression

All micrographs from our IHC staining were analyzed as described above using Metamorph 7.1 image analysis software (Universal Imaging; Downingtown, PA). HIF-1α-, VEGF-, EPO-, ET-1-, MMP-9-, and iNOS- immunopositive-stained retinal cells were identified, quantified, and analyzed. Protein intensities were scored; weak, moderate, or intense.

Molecular Pharmacology Fast Forward. Published on December 14, 2009 as DOI: 10.1124/mol.109.061366
This article has not been copyedited and formatted. The final version may differ from this version.

Glial Cells Culture

R28 cells are immortalized retinal neuoroglial progenitor cells, by transfection with Adenovirus 12S E1A into the neonatal retinal tissue. The cells were a kind gift from Dr. Gail M. Seigel (SUNY, Buffalo, NY). R28 cells express genes characteristic of neurons, as well as functional neuronal properties. R28 cells were cultured in DMEM/F12 medium in a 1:1 mixture, supplemented with 5% FBS, 1.5 mM L-glutamine, 7.5 mM sodium pyruvate, 0.1 mM nonessential amino acids, 1X MEM, 0.37% sodium bicarbonate and 10 μg/ml gentamicin. Cells were incubated at 37°C in the presence of 5% CO_2.

A transformed Müller (glial) cell line (rMC-1) was kindly sent to us by Dr. VJ Sarthy. Müller cell cultures were grown in DMEM supplemented with 15% FBS, as well as with a fungicide mixture and 0.5% gentamicin in a humidified atmosphere of 5% CO_2/95% air. Medium was changed every 2–3 days, and cells were grown to confluence in a 150-mm dish. Cells were split into 60-mm dishes and were used in the experiments when confluent.

In Vitro Hypoxia

Cells were placed in airtight chambers (BioSpherix, Redfield, NY) and the O_2 tension was maintained at 1.2% by using Pro-Ox Model 110 O_2 regulator (BioSpherix, Redfield, NY). The chamber was purged with a gas mixture of 5.32% CO_2, and 93.48% N_2. By employing Trypan Blue Dye Exclusion Assay, we have confirmed that these conditions do not affect viability of the viability of rMC-1 and R28 retinal glial cells (data not shown).

Molecular Pharmacology Fast Forward. Published on December 14, 2009 as DOI: 10.1124/mol.109.061366
This article has not been copyedited and formatted. The final version may differ from this version.

Western Blot

Müller cells (rMC-1) and R28 cells were seeded overnight in 6-well plates (10^5 cells / well). Cells were treated with either YC-1 (25-100 μM) or DMSO (0.2% *v/v*) for 48 hours under normoxic or hypoxic environments. Reactions were terminated by addition of lysis buffer (Cell Signaling, Beverly, MA). Protein content of the cell lysates was determined according to the Bradford method (Bio-Rad, Hercules, CA). Aliquots (40 μg) of whole-cell lysates were separated on 10% SDS-PAGE, and electro-transferred onto polyvinylidene membranes (Amersham Pharmacia Biotech, Little Chalfont). After blocking with 5% nonfat dry milk in TBS-T, the blots were incubated overnight with anti-iNOS and anti-β-actin (internal control) antibodies. Blots were subsequently incubated with peroxidase-conjugated anti-mouse IgG secondary antibody. The signals were obtained by enhanced chemiluminescence (Amersham Biosciences), and visualized by exposure to X-ray film. Upon completion of chemiluminescence, equal lane loading was checked by Ponceau S Solution (Sigma, St. Louis, MO).

Densitometric Analysis of Western Blot

For quantitative evaluation, the bands were subjected to densitometry. X-ray films were scanned with Bio-Rad densitometer (model G-710; Bio-Rad) to quantify band optical density (Quantity One software; Bio-Rad).

Cellular Immunohistochemistry

Müller cells (rMC-1) and R28 cells (2 X 10^4 cells per well) were grown on 8-well chamber slides and cultured in 300 μl of their growing media, which contained YC-1 (25-100 μM) or DMSO

Molecular Pharmacology Fast Forward. Published on December 14, 2009 as DOI: 10.1124/mol.109.061366
This article has not been copyedited and formatted. The final version may differ from this version.

(0.2% *v/v*) and incubated under normoxia or hypoxia for 48 hours at 37°C. YC-1 or DMSO was added 5 minutes prior to the hypoxic incubation. The cells were fixed 48 hours later with 3.7% paraformaldehyde and permeabilized with 0.2% Triton™ X-100 in PBS. The cells were incubated for two hours with anti-iNOS antibody. Negative control experiments consisted of omission of the primary antibody. Cells were then incubated with HRP-conjugate working solution, followed by the addition of the Tyramid solution (TSA Kit#2 and #4 for rMC-1 and R28 staining, respectively) at 1:100 dilutions (Molecular Probes, Carlsbad, CA). Digitized images were acquired utilizing AxioVision software (Zeiss Axiovert 135 and AxioCam). Intensity values of immunofluorescence staining of iNOS in rMC-1 and R28 cells was analyzed and quantified using Metamorph™ imaging analysis software version 7.1 (Universal Imaging, Sunnyvale, CA). The staining intensity in our series ranged from a weak blush to moderate or strong. All Immunocytochemical analyses were measured by Metamorph digital image analysis software (Molecular Devices, Sunnyvale, CA), which was thoroughly described above.

Scoring Assessments of the Cellular Immunohistochemical Analysis for iNOS Expression in rMC-1 and R28 cells

All micrographs from our immunocytochemical staining were analyzed as described above using Metamorph 7.1 image analysis software (Universal Imaging; Downingtown, PA). iNOS-immunopositive-stained retinal cells were identified, quantified, and analyzed. Protein intensities were scored; weak, moderate, or intense.

Molecular Pharmacology Fast Forward. Published on December 14, 2009 as DOI: 10.1124/mol.109.061366
This article has not been copyedited and formatted. The final version may differ from this version.

Statistical Analysis

Analysis of variance using the Kruskal–Wallis test was performed to test for differences in retinopathy score among the various treatment groups. Mann Whitney tests using the Bonferroni method were used to compare the total retinopathy scores and retinopathy subscores. Student's *t*-tests were used to compare the mean number of neovascular nuclei on retinal sections between individual groups. For the analysis of the Real Time RT-PCR data; immunohistochemistry data; Western Blot data, analysis was performed with ANOVA for multiple variables and with *t* – tests. Data are expressed as mean ± SEM from at least 3 independent experiments. Statistical significance was defined as $*P < 0.05; **P < 0.01; ***P < 0.001$.

RESULTS

Double Intravitreous Injections of YC-1 Significantly Reduced Retinopathy in a Mouse Model of OIR

Double injection-regimen of YC-1 (100 μM) were administered intravitreally, immediately after removal from 5-day treatment of 75% oxygen, on P12 and P15. The extent of ischemia-induced retinopathy was first assessed by fluorescein angiography. Retinal angiograms of FITC-dextran injected flat-mounts were evaluated at P12, P15, P17, P21, and P22.

Angiogram of P12 FITC-dextran-perfused retinal flat mounts preparations displays the effects of 5 days of hyperoxic-exposure. P12 retinas exhibit typical signs of central non-perfusion in the center of the retina and a drastic regression in the vascular network, leaving only the major vessels and practically no capillary network (Fig. 1: B1). The peripheral retina still showed evidence of a vascular network, but, in general, the deep vascular plexuses had completely failed to form.

Molecular Pharmacology Fast Forward. Published on December 14, 2009 as DOI: 10.1124/mol.109.061366
This article has not been copyedited and formatted. The final version may differ from this version.

On P12 (Fig. 1: B1), mice were returned to room air (normoxic conditions)**.** As a consequence, a relative hypoxia of ambient atmospheric conditions results in a relative state of ischemia in the poorly vascularized retina, which prompted the excessive re-growth of superficial vessels, and were primarily manifested in the severely hypovascular central retina, causing abnormal vascular growth and quantifiable neovascular response. The term "relative" here refers to an imbalance of the amount of oxygen being delivered to the tissue compared to the amount of oxygen that the tissue needs. In other words, the demand for oxygen exceeds the supply of oxygen. The result is that the tissue becomes hypoxic and does not function at its maximum (or even normal) potential. These pathological conditions are exhibited after return to ambient conditions, because of reduced diffusion of oxygen from the choroid. These pathologic conditions will lead to abnormal sprouting at the interface between retina and vitreous (pre-ILM vascular tufts), angio-proliferation and neovascularization in the immature retina over the next three to five days. These vessels breach the inner limiting membrane into the vitreous in a manner closely resembling retinopathy of prematurity that also shares several characteristics with diabetic retinopathy.

Based on; (1) retinal fluorescein angiography; (2) fluorescent microscopy; and (3) Metamorph™ imaging analysis, our data indicate that between P15 (Fig. 1: B2) and P17 (Fig. 1: B3), approximately 10% to 20% of the total retinal area was covered by neovascular tufts, peaking at P17. These numerous neovascular tufts were seen protruding from the retina into the vitreous. This was evidenced by formation of more and larger neovascular tufts, thickening of the vessels, and heightened staining of the vasculature with the fluorescent dye in these animals when compared with mice raised under ambient conditions.

Molecular Pharmacology Fast Forward. Published on December 14, 2009 as DOI: 10.1124/mol.109.061366
This article has not been copyedited and formatted. The final version may differ from this version.

On P17, non-treated normoxic retinas exhibited virtually complete vascularization of the retina; no avascularized regions, no blood vessel tufts, and the main vessels were straight and showed no dilatation or tortuosity (Fig. 2: A1, A2, A3). However, the vascular network of the O_2-injured retinas and DMSO-treated retinas were significantly altered as demonstrated by an increase in retinal NV (Fig. 2: B1, B2, B3). These retinas displayed the features indicative for a strong ongoing vasoproliferative response: vessel tortuosity and blood vessel tufts. Moreover, these retinas have exhibited avascular regions that arose within the central retina and appeared as dark regions, which were unperfused by fluorescein and occupied 24% and 22% of the size of the total retina, respectively (Figs. 2: B1, B2, B3; yellow arrowheads) and (Fig. 2: C1, C2, C3; yellow arrowheads) as confirmed by a combination of retinal fluorescein angiography, fluorescent microscopy, and Metamorph™ imaging analysis. High-power magnification of the avascular regions demonstrated extensive "popcorn like" neovascular tufts, which were eventually formed within the superficial capillary network of the neovascularized retinas (Fig. 2: B2, B3, C2, C3; red arrowheads). Abnormal pre-retinal neovascular tufts were seen in the mid-periphery, at the interface between the hypovascular central retina and the more vascularized periphery. These neovascular tufts protruded above the inner limiting membrane (ILM) of the retina into the vitreous and often persisted until P21 or later. Furthermore, neovascular lesions from non-treated and DMSO-treated P21 ischemic retinas, exhibited sprouting endothelial cells with multiple filopodia growing at multiple angles at the tips of new vessel spouts, including both along and above the plane of the section (Fig. 5: A1, A2, A3; orange arrowheads).

Angiograms from P22 mice have demonstrated that despite the natural regression of neovascular tufts (Fig. 5: B1, B2, B3) and the healing in the retina; the neovessels, which were

formed by physiological revascularization in non-treated OIR retinas, still appear largely abnormal, as characterized by their tortuosity and several remaining neovascular tufts. Angiograms from P17 mice demonstrated that double intravitreal injection-regimen of YC-1 (100 μM) on P12 and P15 significantly reduced the clinical manifestations of the retinal neovascular response and the retinal vascular tree of these retinas appeared significantly less affected (Fig. 2: D1, D2, D3). In marked contrast, double injection-regimen of DMSO (0.2% *v/v*) on P12 and P15 did not have any influence on the extent of NV (Fig. 2: C1, C2, C3) as compared with YC-1-treated group. YC-1 significantly reduced the cluster area and the number of neovascular tuft formation on P17 (Fig. 2: D1, D2, D3) and on P21 (Fig. 5: C1, C2, C3) as compared with DMSO-treated group. Additionally, YC-1 displayed a statistically significant reduction in the degree of retinopathy, when compared with the DMSO-treated injured retinas (Fig. 2D versus 2C). Furthermore, when compared with the DMSO-treated O_2-injured retinas, YC-1-treated retinas had more preserved and enhanced vasculature on P17 (Fig. 2: D1, D2, D3) and P21 (Fig. 5: C1, C2, C3). DMSO-treated and non-treated ischemic retinas exhibited larger avascular areas, more blood vessel tufts and severe extra-retinal NV, as well as more pronounced retinal vessel tortuosities as compared to YC-1-treated retinas. As confirmed by a combination of retinal fluorescein angiography, fluorescent microscopy, and Metamorph™ imaging analysis; YC-1 treated retinas manifested virtual disappearance of the ischemic areas in the injected eyes, and it significantly decreased the avascular areas by 97% when compared to ischemic controls (Fig. 2: D1, D2, D3). The mean percentage of retinal neovascular response inhibition in the YC-1-treated group as compared with values in the DMSO-treated retinas was 73%.

Molecular Pharmacology Fast Forward. Published on December 14, 2009 as DOI: 10.1124/mol.109.061366
This article has not been copyedited and formatted. The final version may differ from this version.

Effects of YC-1 on Pre-Retinal Neovascular Nuclei

To assess quantitatively the extent of pre-retinal NV, vascular nuclei anterior to the ILM were counted at P17. As expected, in the animals that were grown under ambient conditions, no nuclei were extended into the vitreous (Fig. 3: A1, A2, A3). In marked contrast, all mice, which were exposed to hyperoxia from P7 to P12 and recovered in room air until P17, developed pathologic neovascular tufts extending beyond the ILM into the vitreous (Fig. 3: B1, B2, B3). Treatment of mouse pups with double intravitreal injection-regimen of YC-1 (100 μM) resulted in a significant reduction in pre-retinal nuclei (Fig. 3: D1, D2, D3), when compared to non-treated oxygen-injured retinas (Fig. 3: B1, B2, B3), and significantly less than those in the DMSO treated group (Fig. 3: C1, C2, C3). No neovascular cell nuclei anterior to the internal limiting membrane were observed in the control group maintained in ambient air (normoxia control) (n=8 retinas). In the non-treated oxygen-injured retinas (n=8), the average number of neovascular nuclei extending into the vitreous was (87±4.2), whereas the average number of neovascular nuclei in the DMSO-treated retinas (n=8) was (83±3.7), as compared with (12.65±1.8) nuclei in YC-1-treated mouse retinas (n=8). YC-1 double intravitreal injection-regimen yielded approximately 85.4% and 84.7% reduction of neovascular nuclei anterior to the ILM, as compared with non-treated O_2-injured retinas and the DMSO-treated retinas, respectively (Fig. 4: A) and (Fig. 4: B; Extra Retinal NV).

Assessment of Retinopathy Damage and Severity

The retinopathy scoring criteria (Fig. 4B) measure the retinopathy scores that were obtained from; non-treated normoxic retinas (n=30); non-treated ischemia-injured retinas (n=30); DMSO-treated O_2-injured retinas (n=30); and YC-1-treated O_2-injured retinas (n=30). Lower retinopathy

scores (less retinopathy) represent the status in which the therapeutic modality of YC-1 was highly effective, when compared to the DMSO-treated O_2-injured retinas. The maximal retinopathy score was 13. Non-treated normoxic retinas had a median retinopathy score of 1, compared with non-treated O_2-injured retinas, which scored 12. Pups treated with YC-1 had a median retinopathy score of 3, compared with DMSO-treated ischemic retinas, which scored 11 (Fig. 4C) and (Fig. 7B).

YC-1 Promotes Physiological Revascularization in a Model of Ischemic Retinopathy

To investigate the possible effects of YC-1 on retinal NV, the mouse model of OIR was employed. In order to assess the vascular repair and physiological revascularization mechanisms after hyperoxia-induced obliteration, the obliterated areas were quantified in all animal groups. Mice eyes subjected to this model undergo a reproducible vasodegeneration (P7–12), followed by acute hypoxia (P12–15) leading to aggressive retinal NV (P15–18), which resembles proliferative diabetic retinopathy. Double intravitreal injections of YC-1 promoted vascular repair and significantly enhanced physiological revascularization, compared with non-treated ischemic retinas. At P17, the obliterated areas in YC-1-treated retinas were reduced by 84%, compared with the obliterated areas of non-treated ischemic retinas (Figs. 5: C1, C2, C3 vs. Fig. 1: B3 and Figs. 2: B1, B2, and B3). This was assessed by conducting; (1) retinal fluorescein angiography; (2) fluorescent microscopy, to analyze the retinopathy score; (3) Metamorph™ imaging software, to quantify the extent of retinal NV; (4) Retinal NV scoring as previously described (Higgins et al., 1999). In addition, at P17, the vascular morphology of YC-1 treated retinas appears nearly normal (Figs. 2: D1, D2, D3). The revascularization process was again significantly enhanced in YC-1-treated retinas at P21, and the retinas appeared fully

Molecular Pharmacology Fast Forward. Published on December 14, 2009 as DOI: 10.1124/mol.109.061366
This article has not been copyedited and formatted. The final version may differ from this version.

revascularized (Figs. 5: C1, C2, C3), whereas the delay in the revascularization process was even more apparent in the non-treated ischemic retinas at P17 (Fig. 1: B3 and Figs. 2: B1, B2, and B3). These data demonstrate that YC-1 treatment promotes vascular recovery in the ischemic retina.

OIR Modulates the Vascular Density Profile in the Retinal Microvasculature

Histological analysis of P17 retinal sections stained with endothelial cell–specific antibodies (anti-CD31 and vWF) demonstrated that there was a significant increase in the vascular density [the number of CD31- and vWF-immunopositive endothelial cells per reticle square (100 μm^2)] of YC-1-treated retinas (141.1 ± 3), when compared to the non-treated ischemic retinas (94.2 ± 2), and DMSO-treated group **(**97.1 ± 1) (Fig. 6 and Fig. 7A**).** Therefore, the mean vascular density level of the YC-1-treated group was returned to basal homeostatic level, which was comparable with those of the non-treated normoxic retinas (Fig. 6 and 11A), which displayed a vascular density of (147.4 ± 5). YC-1 concomitantly and significantly enhanced physiological retinal microvascular repair by promoting intra-retinal revascularization. By contrast, DMSO neither inhibited pathological NV nor enhanced RV.

Effects of YC-1 on Gene Expression Levels in the Oxygen-Injured Retinas

To elucidate the molecular mechanisms involved in the regulation of retinal vascularization, the retinal *HIF-1α, VEGF, EPO, ET-1, MMP-9*, and *iNOS* mRNA gene expression levels were evaluated on P17, by quantitative real time RT-PCR. Data were normalized to β-actin mRNA levels. Our data revealed that there were no significant differences between *HIF-1α* message levels of normoxic retinas [Fig. 8A; bar graph 1 (blue)] and non-treated oxygen-injured retinas

Molecular Pharmacology Fast Forward. Published on December 14, 2009 as DOI: 10.1124/mol.109.061366
This article has not been copyedited and formatted. The final version may differ from this version.

[Fig. 8A; bar graph 2 (red)]. Double intravitreal injection-regimen of DMSO (0.2% *v/v*) or YC-1 (100 μM) did not have any influence on *HIF-1α* message levels [(Fig. 8A; bar graph 3 (orange) and bar graph 4 (green), respectively], when compared to non-treated ischemic retinas. Furthermore, data analysis of VEGF, EPO, ET-1, MMP-9 and iNOS mRNA levels exhibited systematic variation in gene expression patterns among various groups of retinal specimens. The minimum gene expression was in the retinas from animals that were placed under ambient conditions, which displayed low gene expression levels [Fig. 8B, 8C, 8D, 8E, and 8F, bar graph 1 (blue)]. In sharp contrast, there was a significant enhancement of *VEGF, EPO, ET-1, MMP-9*, and *iNOS* gene expression levels by the relative hypoxia exposure in the non-treated ischemic retinas, compared with normoxic group [Fig. 8B, 8C, 8D, 8E, and 8F, bar graph 2 (red)]. The effects of sham-treatment on the gene expression patterns paralleled those seen in the non-treated ischemic group [Fig. 8B, 8C, 8D, 8E, and 8F, bar graph 3 (orange)]. Treatment of retinas with YC-1 during the ischemic insult, resulted in significant attenuations in the message levels of *VEGF, EPO, ET-1, MMP-9*, and *iNOS* expressions, compared with non-treated ischemic retinas [Fig. 8B, 8C, 8D, 8E, and 8F, and 8G, bar graph 4 (green)], but their expression level remained slightly higher than that of the non-treated normoxic group.

YC-1 Inhibits HIF-1α, VEGF, EPO, MMP-9, ET-1, and iNOS Protein Levels In Vivo

Non-Treated Normoxic Retinas (Fig. 9) expressed detectable basal levels of HIF-1α in the ganglion cell layer (GCL) and INL. It displayed weak immunoreactivity for VEGF, which was present in the GCL and INL. Furthermore, there was weak to moderate EPO staining that was primarily localized in the neurosensory retina and the GCL. ET-1 was primarily detected in the inner plexiform layer (IPL); whereas weak to moderate staining signals were observed in the

GCL and nerve fibers layer (NFL) (Supplementary Fig. 1). Normoxic retinas also exhibited a very low level of MMP-9 immunoexpression that was detectable in the GCL. iNOS immunostaining revealed very weak but detectable immunoreactivity that was primarily expressed in the GCL.

Non-Treated Oxygen-Injured Retinas (Fig. 9) exhibited the presence of patchy strong HIF-1α overexpression, primarily in the INL and GCL of the ischemic retinas. There was marked elevation of VEGF expression in the NFL and GCL, and to a lesser extent in the IPL of the retinas. VEGF was primarily expressed in the retinal vessels. Additionally, EPO immunoreactivity was up-regulated within the GCL and INL. There was an up-regulation in ET-1 immunoexpression within the GCL, IPL, and INL, as well as strong staining signals, which were localized in the innermost region of the IPL. Furthermore, there was a significant up-regulation of MMP-9 immunoreactivity NFL, GCL, and IPL, which was augmented and localized to the new vessels on the surface of the retina. Moreover, there was a significant increase in the level of iNOS expression in the GCL, IPL, INL. Expression of iNOS was also observed in many of the blood vessels in the NFL. In addition, there was a marked increase of iNOS expression in the outer plexiform layer (OPL), outer nuclear layer (ONL) and outer limiting membrane (OLM) (Supplementary Fig. 1).

DMSO-Treated Oxygen-Injured Retinas (Fig. 9) displayed immunoreactivities that were comparable to those of non-treated O_2-injured retinas. The staining intensity of HIF-1was strong and significantly elevated by 31 folds, when compared with retinas grown under normoxia. In addition, there was a significant up-regulation in VEGF, EPO, ET-1, MMP-9, and iNOS immunoexpressions, when compared to YC-1-treated retinas. There was a significant increase in the level of iNOS expression in the GCL, IPL, INL. iNOS immunolabeling was also markedly

Molecular Pharmacology Fast Forward. Published on December 14, 2009 as DOI: 10.1124/mol.109.061366
This article has not been copyedited and formatted. The final version may differ from this version.

observed in many of the blood vessels in the NFL. There was a marked increase of iNOS expression in the OPL, ONL and the OLM. All proteins manifested an expression pattern that was comparable to the O_2-injured retinas (Supplementary Fig. 1).

In contrast, *YC-1-Treated Oxygen-Injured Retinas* (Fig. 9) displayed a significant down-regulation in HIF-1α and VEGF immunoexpressions. VEGF staining was weak "focal", sporadic and primarily in the GCL region of these retinas. Additionally, EPO and iNOS immunoreactivities were detectable but moderate, and significantly down-regulated compared with DMSO-treated retinas. YC-1 treatment caused a significant inhibition in ET-1 and MMP-9 immunolabelings, compared with DMSO-treated O_2-injured retinas (Supplementary Fig. 1).

YC-1 Inhibits iNOS mRNA Expression Level In Vitro

Since YC-1 appeared to induce physiological revascularization in the OIR model (Figs. 5: C1, C2, C3) and a significant segment of this process seems to occur in the INL, OPL, ONL, and OLM retinal cell layers. Therefore, in view of the fact that glial cells extend from the INL to the OLM, the possibility existed that YC-1 maybe acting directly on retinal glial cells. We therefore, used two cell lines to study the direct effects of YC-1 on iNOS mRNA expression. Real time RT-PCR was employed to examine the presence and the changes of *iNOS* mRNA expression in the two types of cultured cells. After exposure to hypoxia for 48 hours, both rMC-1 cells (Fig. 10A) and R28 cells (Fig. 10B) revealed statistically significant increases in *iNOS* mRNA levels [(Fig. 10: A and B, bar graph 2 (red)], when compared to cells cultured under normoxia, which displayed an extremely low *iNOS* mRNA levels [(Fig. 10: A and B, bar graph 1 (blue)]. Under hypoxia, the expression of iNOS in non-treated r-MC1 and R28 cells had increased 2.3±0.9 and 1.98±0.1 folds, respectively, compared to normoxia where the expression levels were 0.21±0.01

and 0.33±0.01, respectively. Treatment with DMSO did not down-regulate *iNOS* expression [Fig. 10: A and B, bar graph 3 (orange)]. The expression of iNOS in DMSO-treated r-MC1 and R28 cells under hypoxia was 1.98± 0.2 times and 1.96±0.1 times, respectively. Treatment of r-MC1 with 25, 50, 75, and 100 μM YC-1 resulted in a significant dose-dependent inhibition of *iNOS* expression under hypoxia, as compared with the corresponding non-treated hypoxic control cells [(Fig. 10: A; bar graph 4-7 (green)]. In addition, treatment of R28 cell lines with 25, 50, 75, and 100 μM YC-1 resulted in a significant dose-dependent inhibition of *iNOS* expression under hypoxia, as compared with non-treated hypoxic control cells [(Fig. 10B; bar graph 4-7 (green)].

YC-1 Inhibits iNOS Protein Levels in rMC-1 and R28 Cells

Western immunoblot analysis was performed. rMC-1 and R28 cells cultured under normoxia showed extremely low signals of iNOS, while this signal was over-expressed after 48 hours of hypoxic exposure (Fig. 10: C and D; lane 1 versus lane 2, row 1). Western blot analysis indicated that iNOS protein expression was significantly increased, as measured by densitometry, compared to normoxia (Supplementary Fig. 2A and 2B). In both cell types and under hypoxia, YC-1 treatment inhibited the hypoxia-induced iNOS protein levels in a concentration-dependent manner, compared to non-treated hypoxic cells (Fig. 10: C and D; lane 4-7, row 1). In both cell lines, the levels of iNOS began to decrease at 25 μM YC-1, and almost disappeared at 100 μM. In the DMSO-treated cells, iNOS protein levels remained relatively stable under hypoxia, when compared to non-treated cells that were cultured under hypoxia (positive controls) (Fig. 10: C and D; lane 3, row 1). Since YC-1 treatment did not inhibit β-actin, this indicates that YC-1 influence on iNOS protein expression was specific. Direct measurements of protein levels by

Molecular Pharmacology Fast Forward. Published on December 14, 2009 as DOI: 10.1124/mol.109.061366
This article has not been copyedited and formatted. The final version may differ from this version.

Western blot indicated that under hypoxic conditions, iNOS protein expression was significantly increased by 10 fold, compared to normoxia; whereas treatment with 100 μM significantly inhibited iNOS expression by 8 and 9 folds in rMC-1 and R28 cell, respectively, compared to non-treated hypoxic cells, (****P<0.001*) (Supplementary Fig. 2A and 2B).

YC-1 Reduces Fluorescent Immunoreactivity of iNOS Protein in rMC-1 and R28 Cells

Non-treated rMC-1 and R28 cells cultured under hypoxia displayed enriched iNOS protein immunoexpression, with strong staining in the cytoplasms of both cell types (Fig. 11: A and B; Positive Control). Positive controls exhibited significant increase in iNOS protein levels, as compared with cells that were incubated under normoxia, which exhibited limited areas of very weak "blush" iNOS staining (Fig. 11: A and B; negative control). Furthermore, there was a strong positive iNOS staining signals deposited over the cytoplasms of the DMSO-treated cells cultured for 48 hours under hypoxia (Fig. 11: A, and B; DMSO). This intense positive staining was diminished with increasing concentrations of YC-1. No iNOS staining was observed in experiments in which the primary antibody was omitted (data not shown). rMC-1 that were treated with 25 μM YC-1 displayed the presence of cytoplasmic localization but then with weaker equivocal "weak" staining intensity. Whereas, a stronger diffuse cytoplasmic iNOS staining was observed in R28 cells. Our Metamorph quantification analysis have indicated that treatment of rMC-1 and R28 cells with 25 μM YC-1 under hypoxia for 48 hours displayed 60% and 27% inhibition, respectively, compared to non-treated controls cultured under hypoxia (Supplementary Figure 2C and 2D) and (Figure 11). At 50 μM YC-1, iNOS cytoplasmic staining levels was drastically reduced in both cell types, as compared with non-treated controls cultured under hypoxia. Treatment of both cell lines with 50 μM YC-1 for 48 hours under hypoxia caused

Molecular Pharmacology Fast Forward. Published on December 14, 2009 as DOI: 10.1124/mol.109.061366
This article has not been copyedited and formatted. The final version may differ from this version.

a significant inhibition of 70% and 50%, respectively, as compared with non-treated hypoxic controls. At 75 μM YC-1 for 48 hours under hypoxia, YC-1 had significant down-regulatory effects on iNOS protein expression in both cell types, whereas iNOS inhibition in rMC-1 and R28 cells were 80% and 68%, respectively, as compared with non-treated hypoxic controls. At 100 μM, YC-1 displayed significant 85% and 82%folds of inhibition in rMC-1 and R28 cells, respectively, as compared with non-treated hypoxic controls (Supplementary Figure 2C and 2D) and (Figure 11). There were only few stained regions that were still detected in the cytoplasm of YC-1-treated cells.

DISCUSSION

Retinal neovascularization, abnormal formation of new vessels from preexisting capillaries in the retina, is the hallmark of vascular vision-threatening retinal diseases, including diabetic retinopathy, RVO, ROP, and ARMD, which eventually leads to visual loss (Moss *et al*., 1994). There are two distinct types of retinal neovascularization; physiological and pathological. Despite both types of neovascularization stem from retinal ischemia, there is an essential difference in the direction of vessel growth during physiological and pathological neovascularization. In the former, new vessels extend from the optic disc toward the peripheral avascular retina, and follow the guidance of VEGF-expressing retinal astrocytes to compensate for the retinal ischemia (Stone *et al*., 1996). Because simultaneous prevention of both types of retinal NV causes retinal ischemia to be untreated, clinicians await the establishment of new therapeutic modalities that selectively targets pathological neovascularization, while sparing compensatory revascularization. During this investigation, we have chosen P12 and P15 as critical time points to perform our double intravitreal injections-regimen, because, they represent

the hypoxic phase of neovascularization, in addition, around P15 the retinal ischemia initiates an aggressive neovascular response at the interface of the perfused retinal periphery and the ischemic central capillary beds (Medina *et al*., 2008). Furthermore, the model of OIR is widely used to analyze ischemia-induced retinal NV (Smith *et al*., 1994), where exposure to 75% oxygen from P7 to P12 severely disrupts the normal development of the retinal vasculature. When the mice returned to normoxia at P12, relative hypoxia ensued in the severely hypovascular central retina, causing abnormal vascular growth. This is the pathological condition, which induces the release of various angiogenic growth factors, and stimulates pathological vasoproliferation at the junction of the avascular and vascularized retina. Therefore, we have employed the OIR mouse in this study for several reasons; (1) because it is an "ischemia-dependent" model, i.e., the retinas in the OIR mouse model over-express HIF-1 (2) because the OIR mouse model develops retinopathy (retinal neovascularization); (3) because the OIR mouse model exhibits iNOS overexpression.

Data have indicated that attenuation of VEGF activity could effectively suppress retinal NV. Prominent examples of VEGF inhibitors are Avastin and Lucentis. Although antibodies are effective, they are not efficient, because large amounts of these antibodies are needed to suppress the targeted protein, and their inhibitory effects are transient unless these high doses are administered repeatedly. Furthermore, intravitreal injections of VEGF antagonists only partially inhibit retinal NV, suggesting that other growth factors may also participate in the development and progression of retinal NV.

YC-1, a small molecule, has been found to have a novel effect on HIF-1 activity. Specifically, YC-1 reduced the cellular levels of erythropoietin (EPO) and VEGF mRNA in hypoxic Hep3B cells (Chun *et al*., 2001); in addition, YC-1 suppressed the DNA-binding activity

of HIF-1 and HIF-1 protein expression, and reduced HIF-1α accumulation by cobalt or desferrioxamine (Hye-Lim *et al*., 2006). However, since sGC inhibitors failed to block the effects of YC-1 and because 8-bromo-cGMP did not mimic actions of YC-1, the HIF-1-inhibitory effect of YC-1 is probably provided by a novel cellular process linked with the oxygen-sensing pathway (Chun *et al*., 2001). In addition, Yeo *et al*., 2003, have demonstrated that in immunodeficient mice grafted with five kinds of human tumor cells, YC-1 effectively halted tumor growth, and tumors treated with YC-1 showed reduced HIF-1α expression and poor vascularization. In addition, the same study has demonstrated that YC-1 blocked angiogenesis and inhibited tumor growth in mice via suppressing HIF-1α accumulation and inhibiting the expressions of HIF-1-regulated genes, such as VEGF, and glycolytic enzymes in grafted tumors.

In our previous investigation (DeNiro *et al*., 2009), we have demonstrated that YC-1 possesses several anti-angiogenic properties, both *in vitro* and *ex vivo*, which could be exploited as valuable therapeutic potentials to inhibit the formation and growth of new retinal vessels in the hypoxic retina. Previous data have indicated that YC-1 inhibits experimental choroidal NV in rats (Song *et al*., 2008). In this manuscript, we have extended our findings to OIR, *in vivo*, and demonstrated the effectiveness of YC-1 as an anti-angiogenic agent and the role it plays to attenuate the clinical severity and pathogenesis of retinopathy. This study has demonstrated that the hyperoxic "injury" phase prompted specific retinal pathological alterations, which were typical of retinas that have developed and expressed a relentless high degree of vaso-obliteration, central vasoconstriction, as well as absence of central retinal perfusion, increased perfusion at the periphery, persistent dilation and tortuosity of radial vessels. Furthermore, fluorescein angiography has demonstrated that when compared with non-treated oxygen-injured and DMSO treated retinas, YC-1 has reduced major retinopathy alteration criteria that contribute to

pathological NV. These criteria were; (1) the size of the central avascular zones; (2) the number of the total blood neovascular tufts; (3) the extra-retinal NV; and (4) the retinal vessel tortuosity. Additionally, our study has shown that there was a highly significant reduction of ischemic retinopathy in the YC-1-treated retinas compared to DMSO-treated ischemic retinas. The inescapable conclusion is that a dual-injection regimen of YC-1 inhibits the extent of retinopathy. Despite the presence of negligible and minor ischemic pockets; YC-1-treated retinas exhibited a marked evidence of physiological angiogenesis proceeding at the edges of the ischemic area. Histological analysis of P17 retinal sections demonstrated a significant increase in the vascular density of YC-1-treated retinas, when compared to DMSO-treated group**.** The mean vascular density level of the YC-1-treated group returned to a basal homeostatic level, which was comparable with those of the non-treated normoxic retinas. It is therefore tentative to speculate that YC-1 has concomitantly and significantly enhanced physiological retinal microvascular repair by promoting intra-retinal revascularization. Based on the histological appearance of the tissues, no obvious toxic effects, inflammation, or abnormal retinal neuronal or vascular development was detected in retinas of animals receiving YC-1.

Although HIF-1 appears to play a major role in YC-1-mediated effects on retinal NV, other mechanisms are likely to be involved. Previous data have critically demonstrated that there was an increased expression of iNOS immunoreactivity and NO production in the retina of diabetic rats (Carmo *et al*., 2000). Localization of iNOS in the ischemic retina has led to the postulation, which previously demonstrated that the primary effect of iNOS expression is the inhibition of angiogenesis in the ischemic tissue (Sennlaub *et al*., 2001). The same study has demonstrated that iNOS plays a crucial role in retinal neovascular disease by inducing retinal vaso-obliteration and enhancing pathological intravitreal NV. The study also noted that iNOS

deficiency accelerates revascularization of the avascular retina and significantly reduces vitreal invasion and pre-retinal growth. Additionally, data have demonstrated that oxygen-induced retinal vaso-obliteration was significantly reduced by NOS inhibitor, L-nitro-n-arginine (L-NNA), which strongly supports the putative role for NO, in the retinal vaso-obliterative process (Brooks *et al*., 2001).

Previous data have demonstrated that YC-1 inhibits iNOS expression (Pan *et al*., 2005; Hsiao *et al*., 2004), in addition, Lu *et al*., 2007) have demonstrated that YC-1 inhibited LPS-induced production of iNOS and COX-2 in microglia. In this manuscript, during the retinal revascularization process, which was in tandem taking place, neovascular tuft areas were eventually resolved on P17, and ultimately disappeared on P21 in the YC-1 treated retinas, suggesting a novel pleiotropic activities in which YC-1 inhibits pathologic retinal NV, while simultaneously promotes vascular repair and physiological revascularization.

Müller glial cells are specialized radial cells that extend from the INL to the OLM retinal cell layers (Newman and Reichenbach, 1996). Previous data have demonstrated that retinal ischemia induced iNOS expression in Müller cells and retinal ganglion cells (RGCs) (Kobayashi *et al*., 2000). However, Kashiwagi *et al*., (2003) have demonstrated that both retinal glial cells and retinal ganglion cells (RGCs) express three types of NOS-mRNAs, and hypoxia increases NOS-mRNA expression and NO production in retinal glial cells but not in RGCs. Moreover, it has been postulated that the primary effect of iNOS expression is the inhibition of angiogenesis in the ischemic tissue (Sennlaub *et al*., 2001). During this investigation, YC-1 was shown to inhibit iNOS expression in INL, OPL, ONL and ILM. In addition, our *in vitro* studies have revealed that YC-1 directly inhibited iNOS expression at both mRNA and protein levels in retinal neuoroglial cells and Müller cells. Therefore, the possibility exists that under ischemic

conditions, glial cells are the predominant source of iNOS in affected avascular zones of the ischemic retinas, and YC-1 maybe inhibiting iNOS expression by acting directly on retinal glial cells. Our data open the interesting possibility that glial malfunction, may contribute to the breakdown of the blood–retinal barrier in diabetic retinopathy. Taken together, our study demonstrates that the *in vitro* model of hypoxia in the neuoroglial and Müller retinal cells shares common resemblances with the OIR mouse model, because both models exhibit the induction and the accumulation of HIF-1α and the up-regulation of its downstream molecules.

Because pre-retinal growth is the most damaging aspect of retinopathy, this poorly understood event is an attractive therapeutic target. Previous investigations have exhibited that breaching the INL of the retina takes place following hypoxia-induced degeneration of astrocytes, which normally serve as scaffolds for vessels spreading on the retina surface (Stone *et al*., 1996). Other studies (Stellmach *et al*., 2001) have indicated that vitreal invasion takes place upon down-regulation of natural angiogenic inhibitors residing in the vitreous. PEDF, in particular, prevents vessel invasion into avascular compartments of the eye like the vitreous, cornea, and ONL of the retina. Interestingly, VEGF and PEDF are regulated by oxygen in an opposite manner. Hence, the study of Sennlaub *et al* (2001) is consistent with the thesis that pre-retinal growth is elicited whenever the failure to restore retinal normoxia results in a continuous build-up of VEGF in the vitreous. Therefore, these two studies strongly suggest that the balance of pro- and anti-angiogenic activities in the vitreous determine the extent of pre-retinal growth. Taken together, our study has revealed that YC-1 has enhanced the normal vascular development, and promoted a robust vessel regrowth (de novo vessel growth) by inhibiting iNOS expression, as assessed by the retinopathy score, retinal histology and iNOS immunohistochemistry.

Molecular Pharmacology Fast Forward. Published on December 14, 2009 as DOI: 10.1124/mol.109.061366
This article has not been copyedited and formatted. The final version may differ from this version.

Previous investigations have demonstrated that YC-1 stimulates the expression of Heme Oxygenase-1 (HO-1) in vascular SMCs via the PI3K pathway (Liu *et al*., 2009). HO-1 is a cytoprotective, pro-angiogenic and anti-inflammatory enzyme that is strongly induced in injured tissues. The results reported in the present study taken together with the results described above imply that YC-1 may directly sculpt the microenvironment within the vascular plexus—a mechanism that under normal conditions would assure adequate local control of oxygen and nutrient supply. During this study, we found that the mean vascular density level of the YC-1-treated group has returned to a basal homeostatic level, which was comparable with those of the non-treated normoxic retinas. These retinal pathologies appeared to be associated with ischemia and the activation of HIF-1-signaling cascades. These cascades play critical roles in regulating downstream pathways that consequently induce the up-regulation of various growth factors (VEGF, EPO, and ET-1), enzymes (iNOS), and gelatinases (MMP-9).

The formation of new blood vessels or angiogenesis is broadly divided into three phases: vessel destabilization, proliferation/migration and vessel maturation (Carmeliet 2003). When vessel growth is required, the regulatory balance tips toward pro-angiogenic factors. Restoration of steady state is achieved by increasing angiogenesis inhibitors (anti-angiogenic) and vessel stabilization factors. Breakdown of the tightly regulated angiogenic balance leads to abnormal angiogenesis and contributes to a variety of pathological disorders, including cancer, retinal neovascularization, autoimmune conditions, and cardiovascular disease (Carmeliet 2003). Throughout our investigation, YC-1 exhibited pleiotropic effects, which influenced both mechanisms; angiogenesis and vascular repair, via the inhibition of HIF-1α. YC-1 inhibited pathological retinal neovascularization by exhibiting anti-angiogenic activities, which impaired ischemia-induced expression of HIF-1 and its downstream angiogenic molecules, such as VEGF,

EPO, ET-1, leading to the inhibition of NV in the retina. Concomitantly, YC-1 promoted revascularization and exhibited vascular repair properties in the avascular retina by impairing ischemia-induced expression by of HIF-1 and its downstream anti-angiogenic molecules in the avascular retinas, such as iNOS. Our findings may be relevant to the use of intravitreous YC-1 in the management of retinovascular diseases, particularly those with ongoing intraretinal vascular development, such as ROP. There may be a more favorable therapeutic index for YC-1 in treating retinopathy than for an anti-angiogenic agent that suppresses all vessel growth. Our data indicate that YC-1 exerted notable *in vivo* anti-angiogenic effects, which could be exploited as valuable therapeutic potentials to inhibit retinal NV in the ischemic retina.

ACKNOWLEDGMENTS

We thank Dr. Peter Campochiaro, MD (Johns Hopkins University/Wilmer Eye Institute) for his generous support for providing training and technical assistance. Furthermore, we are tremendously grateful to Adara DeNiro for her valuable technical assistance in the quantification of the immunohistochemical and immunocytochemical staining. In addition, we would like to thank Mr. Clive Gray for his seasoned design expertise throughout the various stages of this project. We owe special thanks to Dr. Jörgen Larsson, MD (King Khaled Eye Specialist Hospital) for his detailed, positive and careful review of the manuscript. We also would like to thank Drs. Gail Seigel, PhD (Ross Eye Institute, SUNY, NY) for providing us with R28 cells and Dr. VJ Sarthy, PhD (Northwestern University, Chicago) for providing us with rMC-1 cells.

REFERENCES

Abu El-Asrar AM, Meersschaert A, Dralands L, Missotten L, Geboes K (2004) Inducible nitric oxide synthase and vascular endothelial growth factor are colocalized in the retinas of human subjects with diabetes. *Eye* **18:** 306–313.

Abu El-Asrar AM, Van Damme J, Put W, Veckeneer M, Dralands L, Billiau A & Missotten L (1997) Monocyte chemotactic protein-1 in proliferative vitreoretinal disorders. *American Journal of Ophthalmology* **123:** 599–606.

Adachi K KS, Masai H, Ueda M, Morizane C, Kaneda K, Kume T, Akaike A, Honda Y (1998) Mechanism of the pathogenesis of glutamate neurotoxicity in retinal ischemia. *Graefes Arch Clin Exp Ophthalmol* **10:** 766–774.

Alon T HI, Itin A, Pe'er J (1995) Vascular endothelial growth factor acts as a survival factor for newly formed retinal vessels and has implications for retinopathy of prematurity. *Nat Med* **1:** 1024–1028.

Anonymous (1984) An international classification of retinopathy of prematurity. *Pediatrics* **74:** 127-133.

Aranda JV, Saheb N, Stern L, Avery ME (1971) Arterial oxygen tension and retinal vasoconstriction in newborn infants. *Amer J Dis Child.* **122:** 189-194.

Barinaga M (1995) Shedding light on blindness. *Science* **267:** 452–453.

Borda E, Berra A, Saravia M, Ganzinelli S, Sterin-Borda L (2005) Correlations between neuronal nitric oxide synthase and muscarinic M3/M1 receptors in the rat retina. *Exp Eye Res* **3:** 391–9.

Brooks SE GX, Samuel S, Marcus DM (2001) Reduced severity of oxygen-induced retinopathy in eNOS-deficient mice. *Invest Ophthalmol Vis Sci* **42:** 222–228.

Campochiaro PA (2000) Retinal and choroidal neovascularization. *J Cell Physiol* **184:** 301–310.

Carmeliet P (2003) Angiogenesis in health and disease. *Nat Med* **9:** 653–660.

Carmo A, Cunha-Vaz JG, Carvalho AP, Lopes MC (2000) Nitric oxide synthase activity in retinas from non-insulin-dependent diabetic Goto-Kakizaki rats: correlation with blood–retinal barrier permeability. *Nitric Oxide* **4**: 590–596.

Chakrabarti S, Sima (1997) Endothelin-1 and endothelin-3-like immunoreactivity in the eyes of diabetic and non-diabetic BB/W rats. *Diabetes Res Clin Pract* **37:** 109–20.

Chiou SH CC, Hsu WM, Kao CL, Liu JH, Chen WL, Tsai DC, Wu CC, Chou CK (2001) Elevated nitric oxide level in aqueous humor of patients with acute angle-closure glaucoma. *Ophthalmologica* **215:** 113–116.

Christopherson KS, Bredt DS (1997) Nitric oxide in excitable tissues: physiological roles and disease. *J Clin Invest* **10:** 2424–2429.

Chun YS, Yeo EJ, Choi E, Teng CM, Bae JM, Kim MS, Park JW (2001) Inhibitory effect of YC-1 on the hypoxic induction of erythropoietin and vascular endothelial growth factor in Hep3B cells. *Biochem Pharmacol* **61:** 947–954.

Cross MJ DJ, Matsumoto T, Claesson-Welsh L (2003) VEGF-receptor signal transduction. *Trends Biochem Sci* **28:** 488–494.

Cuzzocrea S, Chatterjee PK, Mazzon E, Dugo L, De Sarro A, Van de Loo FA, Caputi AP, Thiemermann C (2002) Role of induced nitric oxide in the initiation of the inflammatory response after postischemic injury. *Shock* **18:** 169–76.

Das A MA, Song W, McGuire PG (1999) Retinal neovascularization is suppressed with a matrix metalloproteinase inhibitor. *Arch Ophthalmol* **117:** 498–503.

DeNiro M, Alsmadi O, Al-Mohanna F (2009) Modulating the Hypoxia-Inducible Factor Signaling Pathway as a Therapeutic Modality to Regulate Retinal Angiogenesis. *Exp Eye Res* **89:** 700–717.

Du Y SV, Kern TS (2004) Interaction between NO and COX pathways in retinal cells exposed to elevated glucose and retina of diabetic rats. *Am J Physiol Regul Integr Comp Physiol* **287:** 735–741.

Forsythe JA, Jiang BH, Iyer NV, Agani F, Leung SW, Koos RD and Semenza GL (1996) Activation of vascular endothelial growth factor gene transcription by hypoxia-inducible factor 1. *Mol Cell Biol* **16:** 4604–4613.

Fulton D, Gratton JP, McCabe TJ, Fontana J, Fujio Y, Walsh K, Franke TF, Papapetropoulos A, Sessa WC (1999) Regulation of endothelium-derived nitric oxide production by the protein kinase Akt. *Nature* **399:** 597–601.

Galle J, Zabel U, Hübner U, Hatzelmann A, Wagner B, Wanner C, Schmidt HH (1999) Effects of the soluble guanylyl cyclase activator, YC-1, on vascular tone, cyclic GMP levels and phosphodiesterase activity. *Br J Pharmacol* **127:** 195–203.

Hattenbach LO, Falk B, Nurnberger F, Koch FH, Ohrloff C (2002) Detection of inducible nitric oxide synthase and vascular endothelial growth factor in choroidal neovascular membranes. *Ophthalmologica* **216:** 209–214.

He T XY, Zhao XH, Ai M (2007) Interaction between iNOS and COX-2 in hypoxia-induced retinal neovascularization in mice. *Arch Med Res* **8:** 807–815.

Hernández C, Segura RM, Fonollosa A, Carrasco E, Francisco G, Simó R (2005) Interleukin-8, monocyte chemoattractant protein-1 and IL-10 in the vitreous fluid of patients with proliferative diabetic retinopathy. *Diabetic Medicine* **22:** 719–722.

Hierholzer C, Kalff JC, Billiar TR, Bauer AJ, Tweardy DJ, Harbrecht BG (2004) Induced nitric oxide promotes intestinal inflammation following hemorrhagic shock. *Am J Physiol Gastrointest Liver Physiol* **286:** G225–33.

Higgins RD YK, Sanders RJ, Nandgaonkar BN, Rotschild T, Rifkin DB (1999) Diltiazem reduces retinal neovascularization in a mouse model of oxygen induced retinopathy. *Curr Eye Res* **18:** 20–27.

Higgins, RD, Hendricks-Munoz, KD, Caines, VV, Gerrets, RP, Rifkin, DB (1998) Hyperoxia stimulates endothelin-1 secretion from endothelial cells: modulation by captopril and nifedipine. *Curr Eye Res* **17:** 487-493.

Higgins RD, Phelps DL (1990) Oxygen-induced retinopathy: lack of adverse heparin effect. *Ped Res.* **27:** 580–582.

Hsiao G, Huang HY, Fong TH, Shen MY, Lin CH, Teng CM, Sheu JR (2004) Inhibitory mechanisms of YC-1 and PMC in the induction of iNOS expression by lipoteichoic acid in RAW 264.7 macrophages. *Biochem Pharmacol* **67:** 1411–1419.

Hu J, Discher DJ, Bishopric NH, Webster KA (1998) Hypoxia Regulates Expression of the Endothelin-1 Gene through a Proximal Hypoxia-Inducible Factor-1 Binding Site on the Antisense Strand. *Biochem Biophys Res Comm* **3:** 894–899.

Hye-Lim K, Eun-Jin Y, Yang-Sook C, Park JW (2006) A domain responsible for HIF-1α degradation by YC-1, a novel anticancer agent. *International Journal of Oncology* **29:** 255-260.

Inoue A YM, Kimura S, Kasuya Y, Miyauchi T, Goto K, Masaki T (1999) The human endothelin family: three structurally and pharmacologically distinct isopeptides predicted by three separate genes. *Proc Natl Acad Sci USA* **8:** 2863–2867.

Ishida S UT, Yamashiro K, Kaji Y, Amano S, Ogura Y, Hida T, Oguchi Y, Ambati J, Miller JW, Gragoudas ES, Ng YS, D'Amore PA, Shima DT, Adamis AP (2003) VEGF164-mediated inflammation is required for pathological, but not physiological, ischemia-induced retinal neovascularization. *J Exp Med* **198:** 483–489.

Jaquet K, Krause K, Tawakol-Khodai M, Geidel S, Kuck KH (2002) Erythropoietin and VEGF exhibit equal angiogenic potential. *Microvasc Res* **64:** 326–333.

Kashiwagi K, Iizuka Y, Mochizuki S, Tsumamoto Y, Mishima HK, Araie M, Suzuki Y, Tsukahara S (2003) Differences in nitric oxide production: a comparison of retinal ganglion cells and retinal glial cells cultured under hypoxic conditions. *Brain Res Mol Brain Res* **112:** 126–34.

Kaur C, Sivakumar V, Foulds WS (2006) Early response of neurons and glial cells to hypoxia in the retina. *Invest Ophthalmol Vis Sci* **47:**1126–1141.

Ko FN WC, Kuo SC, Lee FY, Teng CM (1994) YC-1, a novel activator of platelet guanylate cyclase. *Blood* **12:** 4226–4233.

Kobayashi M, Kuroiwa T, Shimokawa R, Okeda R, Tokoro T (2000) Nitric oxide synthase expression in ischaemic rat retinas. *Jpn J Ophthalmol* **44:** 235–244.

Kroll J, Waltenberger J (1998) VEGF-A induces expression of eNOS and iNOS in endothelial cells via VEGF receptor-2 (KDR). *Biochem Biophys Res Commun* **252:** 743–746.

Lambert V WB, Munaut C, Galopin C, Jost M, Itoh T, Werb Z, Baker A, Libert C, Krell HW, Foidart JM, Noël A, Rakic JM (2003) MMP-2 and MMP-9 synergize in promoting choroidal neovascularization. *FASEB J* **17:** 2290-2292.

Lambert V, MC, Jost M, Noel A, Werb Z, Foidart JM, Rakic JM (2002) Matrix metalloproteinase-9 contributes to choroidal neovascularization. *Am J Pathol* **161:** 1247-1253.

Lee P WC, Adamis AP (1998) Ocular neovascularization: an epidemiologic review. *Surv Ophthalmol* **3:** 245–269.

Liu XM PK, Mendelev NN, Wang H, Tulis DA, Durante W (2009) YC-1 Stimulates the Expression of Gaseous Monoxide-Generating Enzymes in Vascular Smooth Muscle Cells. *Mol Pharmacol* **75:** 208–217.

Liu Y, Christou H, Morita T, Laughner E, Semenza GL, Kourembanas S (1998) Carbon monoxide and nitric oxide suppress the hypoxic induction of vascular endothelial growth factor gene via the 5′enhancer. *J. Biol. Chem* **273:** 15257–15262.

Liversidge J, Dick A, Gordon S (2002) Nitric oxide mediates apoptosis through formation of peroxynitrite and Fas/Fas-ligand interactions in experimental autoimmune uveitis. *Am J Pathol* **160:** 905–16.

Lu DY, Tang CH, Liou HC, Teng CM, Jeng KC, Kuo SC, Lee FY, Fu WM (2007) YC-1 attenuates LPS-induced proinflammatory responses and activation of nuclear factor-kappaB in microglia. *Br J Pharmacol* **3:** 396–405.

Lush CW, Cepinskas G, Sibbald WJ, Kvietys PR (2001) Endothelial E- and P-selectin expression in iNOS-deficient mice exposed to polymicrobial sepsis. *Am J Physiol Gastrointest Liver Physiol* **280:** G291–7.

Majka S, McGuire P, Colombo S, Das A (2001) The balance between proteinases and inhibitors in a murine model of proliferative retinopathy. *Invest Ophthalmol Vis Sci* **42:** 210–215.

Matsumoto T, Claesson-Welsh L Matsumoto T C-WL (2001) VEGF receptor signal transduction. *Sci STKE* **112:** RE21.

Medina RJ, O'Neill CL, Devine AB, Gardiner TA, Stitt AW (2008) The pleiotropic effects of simvastatin on retinal microvascular endothelium has important implications for ischaemic retinopathies. *PLoS One* **3:** e2584.

Melillo G MT, Sica A, Taylor LS, Cox GW, Varesio L (1995) A hypoxia responsive element mediates a novel pathway of activation of the inducible nitric oxide synthase promoter. *J Exp Med* **6:** 1683–1693.

Mitamura Y, Takeuchi S, Matsuda A, Tagawa Y, Mizue Y & Nishihira J (2001) Monocyte chemotactic protein-1 in the vitreous of patients with proliferative diabetic retinopathy. *Ophthalmologica* **215:** 415–418.

Moss SE, Klein R, Klein BE (1994) Ten-year incidence of visual loss in a diabetic population. *Ophthalmology* **101:** 1061–1070.

Murohara T, Asahara T, Silver M, Bauters C, Masuda H, Kalka C, Kearney M, Chen D, Symes JF, Fishman MC, Huang PL, Isner JM (1998) Nitric oxide synthase modulates angiogenesis in response to tissue ischemia. *J. Clin. Invest* **101:** 2567–2578.

Newman E, Reichenbach A (1996) The Müller cell: a functional element of the retina. *Trends Neurosci* **8:** 307-12.

Nishijima K, Ng YS, Zhong L, Bradley J, Schubert W, Jo N, Akita J, Samuelsson SJ, Robinson GS, Adamis AP, Shima DT (2007) Vascular endothelial growth factor-A is a survival factor for retinal neurons and a critical neuroprotectant during the adaptive response to ischemic injury. *Am J Pathol* **1:** 53-67.

Ozaki H, Seo M S, Ozaki K, Yamada H, Yamada E, Okamoto N, Hofmann F, Wood J M, Campochiaro P A (2000) Blockade of vascular endothelial cell growth factor receptor signaling is sufficient to completely prevent retinal neovascularization. *Am J Pathol* **2:** 697-707.

Ozaki H, Yu A Y, Della N, Ozaki K, Luna J D, Yamada H, Hackett S F, Okamoto N, Zack D J, Semenza G L, Campochiaro P A (1999) Hypoxia inducible factor-1alpha is increased in ischemic retina: temporal and spatial correlation with VEGF expression. *Invest Ophthalmol Vis Sci* **1:** 182-9.

Palmer, L.A., Semenza, G.L., Stoler, M.H., and Johns, R.A (1998) Hypoxia induces type II NOS gene expression in pulmonary artery endothelial cells via HIF-1. *Am. J. Physiol* **274:** L212–L219.

Pan SL, Guh JH, Peng CY, Chang YL, Cheng FC, Chang JH, Kuo SC, Lee FY, Teng CM (2005) A potential role of YC-1 on the inhibition of cytokine release in peripheral blood mononuclear leukocytes and endotoxemic mouse models. *Thromb Haemost* **5:** 940-8.

Papapetropoulos A, Garcia-Cardena G, Madri JA, Sessa WC (1997) Nitric oxide production contributes to the angiogenic properties of vascular endothelial growth factor in human endothelial cells. *J Clin Invest* **100:** 3131–3139.

Parenti A, Morbidelli L, Cui XL, Douglas JG, Hood JD, Granger HJ, Ledda F, Ziche M (1998) Nitric oxide is an upstream signal of vascular endothelial growth factor-induced extracellular signal-regulated kinase1/2 activation in postcapillary endothelium. *J Biol Chem* **273:** 4220–4226.

Pe'er J SD, Itin A, Hemo I, Gnessin H, Keshet E (1995) Hypoxia-induced expression of vascular endothelial growth factor by retinal cells is a common factor in neovascularizing ocular diseases. *Lab Invest* **6:** 638–645.

Phelps, DL, Rosenbaum A (1984) Effects of marginal hypoxemia on recovery from oxygen-induced retinopathy in the kitten model. *Pediatrics* **73:** 1–6.

Phelps DL, Rosenbaum AL (1977) The role of tocopherol in oxygen-induced retinopathy: kitten model. *Pediatrics* **59:** 998–1005.

Pierce EA AR, Foley ED, Aiello LP, Smith LEH (1995) Vascular endothelial growth factor/vascular permeability factor expression in a mouse model of retinal neovascularization. *Proc Natl Acad Sci USA* **92:** 905–909.

Pipili-Synetos E, Kritikou S, Papadimitriou E, Athanassiadou A, Flordellis C, Maragoudakis ME (2000) Nitric oxide synthase expression, enzyme activity and NO production during angiogenesis in the chick chorioallantoic membrane. *Br J Pharmacol.* **129:** 207–213.

Qi X, Sarthy V.P., Penn J.S (2004) VEGF Induction by Hypoxia in Muller cells. *Invest Ophthalmol Vis Sci*: ARVO E-Abstract #1887.

Rajendram R, Saraswathy S, Rao NA (2007) Photoreceptor mitochondrial oxidative stress in early experimental autoimmune uveoretinitis. *Br J Ophthalmol* **91:** 531–7.

Salani D, Taraboletti G, Rosanò L, Di Castro V, Borsotti P, Giavazzi R, Bagnato A (2000) Endothelin-1 induces an angiogenic phenotype in cultured endothelial cells and stimulates neovascularization *in vivo*. *Am J Pathol* **5:** 1703-11.

Semenza GL (2000) Expression of hypoxia-inducible factor 1: mechanisms and consequences. *Biochem Pharmacol* **59:** 47–53.

Sennlaub F CY, Goureau O (2001) Inducible nitric oxide synthase mediates the change from retinal to vitreal neovascularization in ischemic retinopathy. *J Clin Invest* **107:** 717–725.

Sennlaub F, Courtois Y, Goureau O (1999) Nitric oxide synthase-II is expressed in severe corneal alkali burns and inhibits neovascularization. *Invest Ophthalmol Vis Sci* **40:** 2773–2779.

Sivak JM, Fini ME (2002) MMPs in the eye: emerging roles for matrix metalloproteinases in ocular physiology. *Prog Retin Eye Res* **1:** 1–14.

Smith LE, Wesolowski E, McLellan A, Kostyk SK, D'Amato R, Sullivan R, D'Amore PA (1994) Oxygen-induced retinopathy in the mouse. *Invest Ophthalmol Vis Sci* **35:** 101–111.

Song Sj, Chung H, Yu HG (2008) Inhibitory effect of YC-1, 3-(5'-hydroxymethyl-2'-furyl)-1 benzylindazole, on experimental choroidal neovascularization in rat. *Ophthalmic Res* **40:** 35–40.

Steen B SS, Berglin L, Seregard S, Kvanta A (1998) Matrix metalloproteinases and metalloproteinase inhibitors in choroidal neovascular membranes. *Invest Ophthalmol Vis Sci* **39:** 2194–2200.

Stellmach, V., Crawford, S.E., Zhou, W., and Bouck, N (2001) Prevention of ischemia-induced retinopathy by the natural ocular antiangiogenic agent pigment epithelium-derived factor. *Proc. Natl. Acad. Sci. USA* **98:** 2593–2597.

Stone J, Chan-Ling T, Itin A, Gnessin H, Keshet E (1996) Roles of vascular endothelial growth factor and astrocyte degeneration in the genesis of retinopathy of prematurity. *Invest Ophthalmol Vis Sci* **37:** 290–299.

Tadesse M, Yan Y, Yossuck P, Higgins RD (2001) Captopril improves retinal neovascularization via endothelin-1. *Invest Ophthalmol Vis Sci* **8:** 1867-72.

Takagi C, Bursell SE, Lin YW, Takagi H, Duh E, Jiang Z,Clermont AC, King GL (1996) Regulation of retinal hemodynamics in diabetic rats by increased expression and action of endothelin-1. *Invest Ophthalmol Vis Sci* **37:** 2504–2518.

Teng CM, Wu CC, Ko FN, Lee FY, Kuo SC (1997) YC-1, a nitric oxide-independent activator of soluble guanylate cyclase, inhibits platelet-rich thrombosis in mice. *Eur J Pharmacol* **320:** 161–166.

Thillaye-Goldenberg B, Goureau O, Naud MC, de Kozak Y (2000) Delayed onset and decreased severity of experimental autoimmune uveoretinitis in mice lacking nitric oxide synthase type 2. *J Neuroimmunol* **110:** 31–44.

Tsurumi Y, Murohara T, Krasinski K, Chen D, Witzenbichler B, Kearney M, Couffinhal T, Isner JM (1997) Reciprocal relation between VEGF and NO in the regulation of endothelial integrity. *Nat. Med* **3:** 879–886.

Tuder, R.M., Flook, B.E., and Voelkel, N.F (1995) Increased gene expression for VEGF and the VEGF receptors KDR/Flk and Flt in lungs exposed to acute or to chronic hypoxia. Modulation of gene expression by nitric oxide. *J. Clin. Invest* **95:** 1798–1807.

Van der Zee R, Murohara T, Luo Z, Zollmann F, Passeri J, Lekutat C, Isner JM (1997) Vascular endothelial growth factor/vascular permeability factor augments nitric oxide release from quiescent rabbit and human vascular endothelium. *Circulation* **95**: 1030–1037.

Wang GL, Semenza G (1996) Molecular basis of hypoxia-induced erythropoietin expression. *Curr Opin Hematol* **3**: 156–162.

Watanabe D SK, Matsui S, Kurimoto M, Kiryu J, Kita M, Suzuma I, Ohashi H, Ojima T, Murakami T, Kobayashi T, Masuda S, Nagao M, Yoshimura N, Takagi H (2005) Erythropoietin as a retinal angiogenic factor in proliferative diabetic retinopathy. *N Engl J Med* **353**: 782–792.

Yamada H, Yamada E, Hackett SF, Ozaki H, Okamoto N, Campochiaro PA (1999) Hyperoxia causes decreased expression of vascular endothelial growth factor and endothelial cell apoptosis in adult retina. *J Cell Physiol* **179:** 149-56.

Yeo CY, Cho YS, Kim J, Lee JC, Kim MS, Park JW (2003) YC-1: a potential anticancer drug targeting hypoxia-inducible factor 1. *J Natl Cancer Inst* **95**: 516–525.

Zhang X, Sakamoto T, Hata Y, Kubota T, Hisatomi T, Murata T, Ishibashi T, Inomata H (2002) Expression of matrix metalloproteinases and their inhibitors in experimental retinal ischemia-reperfusion Injury in rats. *Exp Eye Res* **74:** 577–584.

Ziche M, Morbidelli L, Choudhuri R, Zhang HT, Donnini S, Granger HJ, Bicknell R (1997) Nitric oxide synthase lies downstream from vascular endothelial growth factor-induced but not basic fibroblast growth factor-induced angiogenesis. *J Clin Invest* **99:** 2625–2634.

Molecular Pharmacology Fast Forward. Published on December 14, 2009 as DOI: 10.1124/mol.109.061366
This article has not been copyedited and formatted. The final version may differ from this version.

FIGURE LEGENDS

FIG. 1

A. Timeline of Study of Retinal Vasculature during Normal Development and Oxygen-Induced Retinopathy

This diagram was based on the protocol, which was developed by Smith *et al*. (1994) [**66**]. Experimental mice were placed in 75% O_2 between P7 and P12. Mice were returned to room air on P12, which triggered a relative ischemic condition in the retina. The retina then exhibited pathologic growth of vessels in the superficial layer; with pre-retinal vascular tufts that extended through the ILM into the vitreous. Double intravitreal injections of YC-1 (100 μM) were injected, immediately after removal from 5-day treatment of 75% oxygen, on P12 and P15. Mice were sacrificed on P12, P15, P17, P21, and P22. *Solid Blue Line*, normal vessel growth under ambient conditions; *Solid Red Line*, vessel growth under OIR conditions; *Needles*, YC-1-injections time points.

B1. Image represents non-treated OIR retina at P12 (n=4); Retinas prepared from P12 exhibited marked regression of the central vascular network (yellow arrowheads) after exposure to 75% oxygen at P7.

B2. Image represents non-treated OIR retina at P15 (n=4); Retinas prepared from P15 displayed the loss of central vasculature (yellow arrowheads) and the presence of tortuous blood vessels (orange arrowheads).

B3. Image represents non-treated OIR retina at P17 (n=8); Retinas prepared from P17 showed partial revascularization from the periphery inward after return to normoxic conditions at P12, accompanied by the formation of pathologic new vascular tufts (red arrowheads). Please not the avascular area (yellow arrowheads) in the central segment of the retina and the presence of severe vessel tortuosity (orange arrowheads).

FIG. 2

Quantitative Assessment of NV in P17 Mice Exposed to a Cycle of Hyperoxia and Room Air (OIR)

Panels (A, B, C, and D). Representative images of whole-mount retina preparations on P17 of different mice groups.

A. Retina from P17 "control" room air-reared mouse (n=22 retinas) shows a homogeneous normal delicate vessel pattern throughout the retina. The retina is completely vascularized without avascularized areas. No blood vessel tufts are present. The main vessels show no tortuosity and no dilation. Certain portions (A2 and A3) of the image were enlarged (white frames).

B. Retina from P17 non-treated oxygen-injured group (n=8 retinas) shows an engorged tortuous appearance of the blood vessels, large central avascular area (yellow arrows), and high presence of blood vessel tufts (red arrows). Certain portions of the neovascular regions (B2 and B3) of the image were enlarged (white frames).

Molecular Pharmacology Fast Forward. Published on December 14, 2009 as DOI: 10.1124/mol.109.061366
This article has not been copyedited and formatted. The final version may differ from this version.

C. Retina of oxygen-exposed mouse that was injected with the DMSO, immediately after removal from 5-day treatment of 75% oxygen, on P12 and P15 and sacrificed on P17 (n=11). The retinas show profound vascular engorgement with apparent vaso-obliteration and neovascular tuft formation. The avascularized area has the same size after injection of the vehicle. The size of the central avascularized areas remained almost unaffected by DMSO. Certain portions (C2 and C3) of the neovascular and vaso-obliterated regions were enlarged (white frames).

D. Retina from P17 mice that have undergone the oxygen-induced model of retinopathy, subsequently given double injections of YC-1 on P12 and P15, and later sacrificed on P17 (n=11). The retinas display a normal vascular pattern similar to (A). When compared to non-treated ischemic retinas, the structure of the retinal vasculature was significantly better preserved; the avascularized areas and the growth of new vascular tufts were significantly decreased after a double intravitreal injection-regimen of YC-1. Certain portions of normal vascular pattern (D2 and D3) of the image were enlarged (white frames). Please note that there is a significant decrease in the degree of retinal NV in YC-1-treated retina compared with non-treated oxygen-injured and DMSO-treated mice (***$P < 0.001$). Scale bars: A1, B1, C1, and D1= 200 μm; A2, A3, B2, B3, C2, and C3 = 100 μm.

FIG. 3

YC-1 Suppresses the Development and Progression of Pathological Retinal NV

H&E–stained cross section from the retina of a mouse exposed to 75% oxygen for 5 days followed by room air for additional 5 days. Neovascular tufts were confirmed by extending into

Molecular Pharmacology Fast Forward. Published on December 14, 2009 as DOI: 10.1124/mol.109.061366
This article has not been copyedited and formatted. The final version may differ from this version.

the vitreous (marked with circles). Retinal NV determined by counting the number of retinal neovascular cell nuclei anterior to the ILM on P17. The double intravitreal injection- regimen of YC-1 shows a significant reduction of the number of retinal neovascular cell nuclei (D), when compared with the non-treated ischemic group (B) and the DMSO-injected ROP group (C), but more than that of the non-treated normoxic group (A). Tissue sections were visualized at 63X and 200X (original magnification). These experiments were repeated at least three times with eyes from five P17 mice (n=8 retinas per group). Scale bars: A1, B1, C1, and D1 (200 μm); A2, A3, B2, B3, C2, C3, D2, D3 (500 μm).

FIG. 4

A. Histological Analysis of Ischemia-Induced NV of the Mouse Retina

Extra-retinal nuclei count from retinal sections. The blue bar graph represents the mean number of extra-retinal neovascular nuclei in room air-reared animals. The red bar graph represents the mean number of extra-retinal neovascular nuclei in 75% O_2 – exposed animals. The orange bar graph represents the mean number of extra-retinal neovascular nuclei in DMSO-treated animals. The green bar graph represents the mean number of extra-retinal neovascular nuclei in YC-1-treated animals. Pre-retinal nuclei were counted in a masked fashion. Intravitreal injection of YC-1 significantly reduced (**$P < 0.01$) the number of pre-retinal nuclei by 85.45% in comparison to non-treated ischemic control retinas. There was no statistically significant difference between non-treated ischemic controls and DMSO-treated retinas. Data in each bar are the mean number of vascular cell nuclei in four mice (8 retinas per group).Values are presented as mean ± S.E.M. Statistical significance was analyzed using ANOVA.

B. Scoring System to Assess the Severity of Retinopathy in Oxygen-Induced Retinal Damage

The retinopathy scoring criteria measure the retinopathy scores that were obtained from all four groups. Lower retinopathy scores (less retinopathy) represent the status in which the therapeutic modality of YC-1 was highly effective, when compared to the DMSO-treated O_2-injured retinas. The maximal retinopathy score was 13. Non-treated normoxic retinas had a median retinopathy score of 1, compared with non-treated O_2-injured retinas, which scored 12 (**$P < 0.01$). Pups treated with YC-1 had a median retinopathy score of 3, compared with DMSO-treated ischemic retinas, which scored 11 (**$P < 0.01$).

C. Subcategories of the Retinopathy Scoring System

Blue bar graph represents the average retinopathy score of room air-reared mice. Red bar graph represents the average retinopathy score of mice exposed to 75% oxygen. Orange bar graph represents the average retinopathy score of mice exposed to 75% oxygen, and immediately after removal from 5-day treatment of 75% oxygen, they were injected on P12 and P15 with DMSO. Green bar graph represents the average retinopathy score of mice exposed to 75% oxygen and immediately after removal from 5-day treatment of 75% oxygen, they received a double-intravitreal injection regimen of YC-1 (100 μM) on12 and P15. A significant decrease of central avascular area, neovascular tufts, extra-retinal NV, and vessel turtuosity, by double intravitreal injection regimen of YC-1. Please note the increase of the avascularization area, proliferative neovascular tufts, extra-retinal NV, and vessel turtuosity in the non-treated ischemic retinas. Intravitreal injection of the vehicle, DMSO, on P12 and P15 did not have a significant impact on the level of NV. Data in each bar are the mean non-perfused area relative to whole area of each retina in 15 mice (30 retinas per group). Values are presented as mean ± S.E.M. (**$P < 0.01$).

Molecular Pharmacology Fast Forward. Published on December 14, 2009 as DOI: 10.1124/mol.109.061366
This article has not been copyedited and formatted. The final version may differ from this version.

FIG. 5

Qualitative Assessment of NV in Whole-Mount Retinas at Different Phases of Progression through the OIR Model

All mice were exposed to a cycle of hyperoxia and room air (OIR), and later were perfused with fluorescein dextran. Retinal vessels at different stages present different vasculature pattern from the normal retina. Each fluorescence image was collected using X20 and X100 objective lens.

(A1, A2, A3). Characterization of the Endothelial Tip Cell Filopodia in the OIR Mouse Model

High power resolution imaging of P17-fluorescein dextran–stained retinas revealed that neovascular areas exhibit sprouting endothelial cells that project numerous long filopodia (marked with orange arrowheads), which were seen at sprouting tips of new vessel sprouts in the deeper retinal plexus, and were uniform in thickness (~100 nm) but of variable length, with an average length extending 20-30 μm, with the longest extending <100 μm. (100X objective).

(B1, B2, and B3). Images represent non-treated OIR retinas at P22 (n=6); revascularization of the retina is largely complete by P22, but resolving areas of NV in fluorescein dextran-stained retina demonstrate that tufts were diminishing (red arrowheads), but the retinal vasculature was still abnormal, while vessels tortuosity (orange arrowheads) and the presence of central avascular zones (yellow arrowheads) still persist. Certain portions (B2 and B3) of the avascular, neovascular and vaso-obliterated regions were enlarged (white frames).

(C1, C2, and C3). Images represent YC-1-treated OIR retina at P21 (n=11); Images demonstrate the dissolution of neovascular tufts and the complete disappearance of central avascular zones

(inhibition of retinal NV). Despite the presence of a very mild tortuosity of the retinal vessels (orange arrowheads)**,** there was a significant growth and formation of new and healthy vessels (physiological RV) that occupied the entire retina. YC-1 enhanced the process of faster retinal revascularization as demonstrated by a reduction in the area of obliteration, compared with non-treated ischemic retina. The vasculature in OIR retinas treated with YC-1 looked relatively normal and lacked the characteristic of severe tortuosities, which was one of the clinico-pathological features of revascularized regions in non-treated OIR retinas. Scale bar is 200 μm for (A1, B1, and C1); and 100 μm for (A2, A3, B2, B3, C2, and C3). Certain portions (C2 and C3), which exhibit the therapeutic impact of YC-1 on the treated retinas were enlarged (white frames).

FIG. 6

A. Quantification of Vascular Densities in Normoxic, Non-Treated Ischemic, Vehicle-Treated Ischemic and Drug-Treated Ischemic Retinas

We quantified the numbers of vWF-immunoreactive vessels (left column) and the CD31-immunopositive vessels (right column) in P17 retinal sections from normoxic (blue blocks), non-treated ischemic (red blocks), DMSO-treated (orange blocks), and YC-1-treated retinas (green blocks). There was a significant decrease in the vascular density [the number of CD31- and vWF-immunopositive endothelial cells per reticle square (100 μm^2)] of non-treated oxygen-injured retinas (***P<0.01*) and DMSO-treated group (***P<0.01*)**,** when compared with non-treated normoxic control group. The mean vascular density level of the YC-1-treated group was returned to basal homeostatic level, which was comparable with those of the non-treated normoxic retinas.

Molecular Pharmacology Fast Forward. Published on December 14, 2009 as DOI: 10.1124/mol.109.061366
This article has not been copyedited and formatted. The final version may differ from this version.

FIG. 7

A. Number of endothelial cells per reticle square (100 μm^2) in Normoxic, Non-Treated Ischemic, Vehicle-Treated Ischemic and Drug-Treated Ischemic Retinas

Histological analysis of retinal sections stained with anti-CD31 on P17 demonstrated that there was a significant increase (***P<0.01*) in the vascular density [the number of CD31-immunopositive endothelial cells per reticle square (100 μm^2)] of YC-1-treated retinas, as compared to the non-treated ischemic retinas and DMSO-vehicle group, which both displayed a significant decrease in the vascular density. The mean vascular density level of the YC-1-treated group was returned to basal homeostatic level, which was comparable with those of the non-treated normoxic retinas.

B. Total Retinopathy Scores in the Normal and the Experimental OIR Groups Animals (P17) treated with YC-1 after hyperoxia had significantly less total retinopathy scores than oxygen-injured retinas. Average retinopathy score of room air-reared mice (blue bar graph). Average retinopathy score of mice exposed to 75% oxygen (red bar graph). Average retinopathy score of mice exposed to 75% oxygen that had double-injections of DMSO (orange bar graph). Average retinopathy score of mice exposed to 75% oxygen and had a double-injection regimen of YC-1 (100 μM) on P12 and P15 (green bar graph). (****P*<0.001) and (***P* < 0.01), as compared to DMSO-treated ischemic control.

Molecular Pharmacology Fast Forward. Published on December 14, 2009 as DOI: 10.1124/mol.109.061366
This article has not been copyedited and formatted. The final version may differ from this version.

FIG. 8

YC-1 does not Influence Retinal HIF-1α Transcriptional Level, While it Inhibits Retinal VEGF, EPO, ET-1, MMP-9, and iNOS mRNA Expression, In Vivo

(A, B, C, D, E, and F). Relative amount of VEGF, MMP-9, and iNOS mRNAs in the retinas of normoxic and OIR experimental animals as measured by real-time PCR. In mice that were raised under ambient conditions, retinal HIF-1α mRNA was detected at very low level. On P17, and after exposure to relative hypoxia for 5 days, there was a negligible up-regulation in HIF-1α mRNA levels (red bar graph), when compared with the normoxic controls (blue bar graph). Treatment of mice with 25, 50, 75, and 100 μM YC-1, did not have any influence on HIF-1α mRNA expression levels, when compared with ischemic controls (green bar graph vs. red bar graph). Furthermore, the mRNA levels of VEGF, EPO, ET-1, MMP-9, and iNOS were increased in the non-treated ischemic retinas (red bar graphs), while non-treated normoxic retinas exhibited extremely low mRNA levels (blue bar graphs). Treatment of ischemic retinas with 100 μM YC-1 resulted in a significant inhibition of VEGF (***P<0.001), EPO (***P<0.001), ET-1 (**P<0.01), MMP-9 (**P<0.01), and iNOS (***P<0.001) mRNA expression (green bar graphs). The message levels of VEGF, EPO, ET-1, MMP-9, and iNOS, display an efficient and significant knockdown of genes expression after double intravitreal injection-regimen of 100 μM YC-1, as compared to non-treated ischemic retinas. ANOVA was used for statistical analyses. Mean ± SEM of mRNA level normalized to β-actin were calculated, (***P<0.001) and (**P < 0.01), as compared to non-treated ischemic control. Data are representative of 3 independent experiments.

G. Sequence for Molecular Beacons and the Primer Used for the Quantitative Real-Time PCR Analysis.

Molecular Pharmacology Fast Forward. Published on December 14, 2009 as DOI: 10.1124/mol.109.061366
This article has not been copyedited and formatted. The final version may differ from this version.

FIG. 9

Immunohistochemical Analysis for Retinal HIF-1α, VEGF, EPO, ET-1, MMP-9, and iNOS Expression in Mice with Oxygen-Induced Retinopathy

Representative photomicrographs of retinas from various OIR groups that were immunostained for HIF-1α, VEGF, EPO, ET-1, MMP-9, and iNOS. The expression of HIF-1α, VEGF, EPO, ET-1, MMP-9, and iNOS was up-regulated in the non-treated ischemic and DMSO-treated groups, compared with non-treated normoxic group. Whereas, all protein immunoreactivities were down-regulated in the YC-1-treated group, compared with non-treated ischemic and DMSO-treated groups. Retinas were examined at X60 objective. Scale bar: 500 μm.

FIG. 10

YC-1 Induces a Significant Down-Regulation of iNOS Gene Expression and Protein Levels, In Vitro

(A) and (B). The mRNAs were isolated, and *iNOS* mRNA levels were measured by quantitative real time RT-PCR. The expression profile of iNOS-mRNA significantly changed in rMC-1 and R28 cells. The expression of iNOS was significantly increased at 48 hours post-hypoxic incubation. DMSO-treatment did not have any influence on iNOS message level. YC-1-treatment caused a significant dose-dependent down-regulation of iNOS-mRNA expression in both cell lines. ANOVA tests were used for the analyses. $^{**}P<0.01$ (50, 75, and 100 μM YC-1 vs. non-treated positive control), and $^{*}P < 0.05$ (25 μM vs. non-treated positive control. Data are representative of 3 independent experiments. Values are presented as mean ± S.E.M.

Molecular Pharmacology Fast Forward. Published on December 14, 2009 as DOI: 10.1124/mol.109.061366
This article has not been copyedited and formatted. The final version may differ from this version.

(C) and (D). Western immunoblot analysis using rabbit anti-iNOS polyclonal antibody was performed on total protein extracts from rMC-1 and R28 cells cultured under normoxic or hypoxic conditions, and were either left untreated, or treated under hypoxia with DMSO (0.2% *v/v*), or YC-1 (25-100 μM) for 48 hours. β-actin was used as a control protein. Lane 1 indicates normoxic controls; Lane 2 indicates hypoxic controls; Lanes 4 indicates DMSO-treated cells under hypoxic conditions; Lane 4 to 7 indicate YC-1-treated group under hypoxia. All signals were quantitated and normalized against β-actin measurements. Data are representative of 3 independent experiments. Protein expression levels were elevated markedly in the non-treated hypoxic cells. In YC-1-treated hypoxic cells, iNOS protein expression was significantly decreased in a dose-dependent fashion, compared with non-treated hypoxic cells (r-MC-1 and R28). Statistical significance was determined by ANOVA (**P<0.01).

FIG. 11

Immunofluorescence Analysis of iNOS Expression, In Vitro

Photomicrographs showing immunofluorescence analysis of (A) Müller cells (rMC-1), or (B) R28 cells. Cells were incubated for 48 hours with DMSO (0.2% *v/v*) under normoxic (blue blocks) (negative control) or hypoxic conditions (red blocks) (positive control). In different wells, cells were treated with either DMSO (orange blocks) or YC-1 (25, 50, 75 and 100 μM) (green blocks), and incubated under hypoxic conditions for 48 hours. The cells were subsequently fixed for immunocytochemistry. The cells were immunocytochemically stained with rabbit anti-iNOS polyclonal antibody. The signal was detected using Tyramid working solution [TSA Kit#2 (green)] for rMC-1 staining, and [TSA Kit#4 (red)] for R28 staining. Intense staining was considered a positive signal. Yellow arrows indicate rMC-1 and R28 cells

over-expressing iNOS. Under hypoxic conditions, non-treated hypoxic cells exhibited extremely high iNOS immunoreactivity. There was a strong iNOS-positive staining signals of iNOS deposited over the cytoplasms and nuclei of the DMSO-treated cells incubated under hypoxia. Treatment of cells with various concentrations of YC-1 under hypoxic conditions for 48 hours resulted in a dose- dependent inhibition of iNOS expression. Images are representatives of three independent experiments. Scale bars, 0.3 mm.

Molecular Pharmacology Fast Forward. Published on December 14, 2009 as DOI: 10.1124/mol.109.061366
This article has not been copyedited and formatted. The final version may differ from this version.

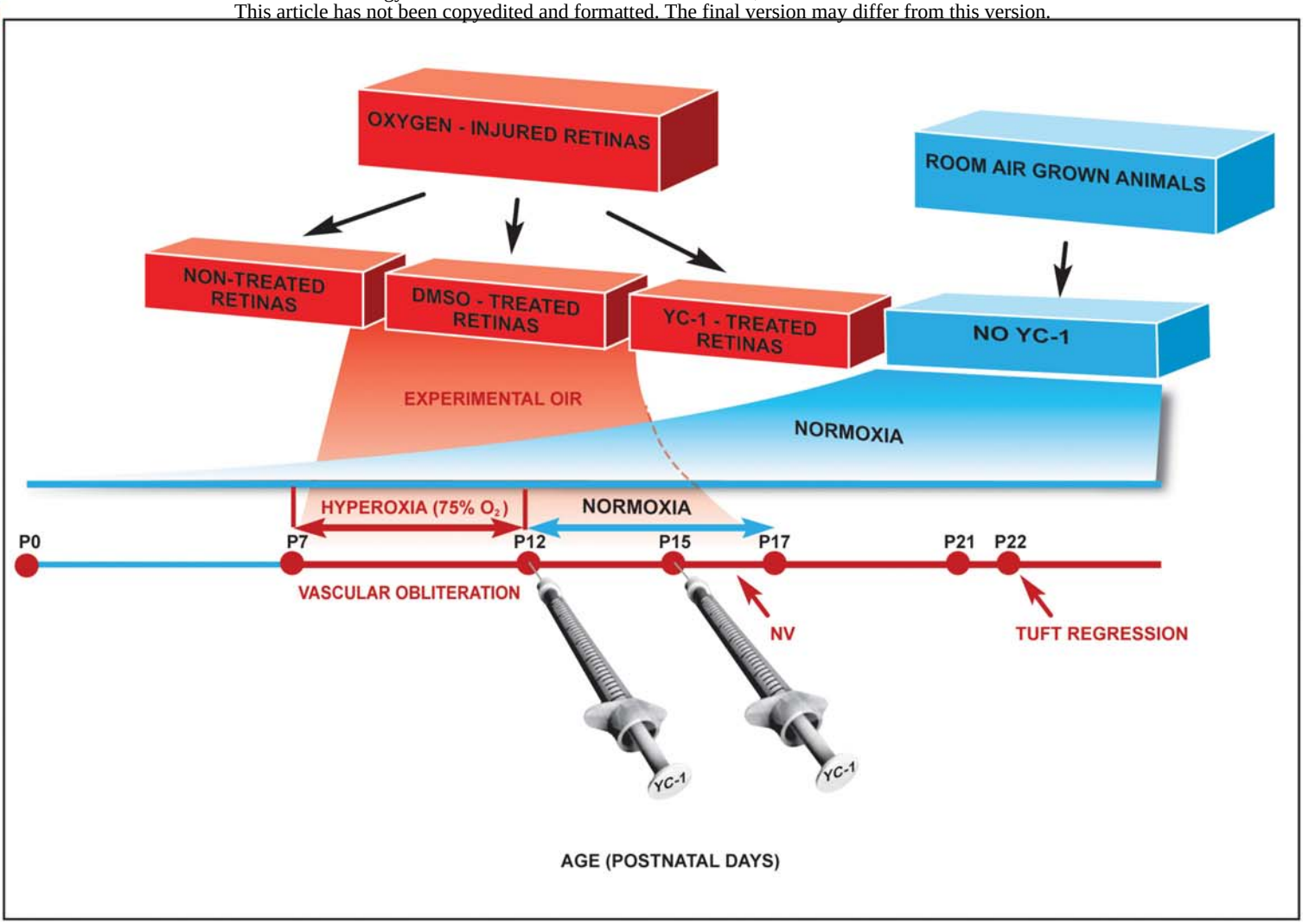

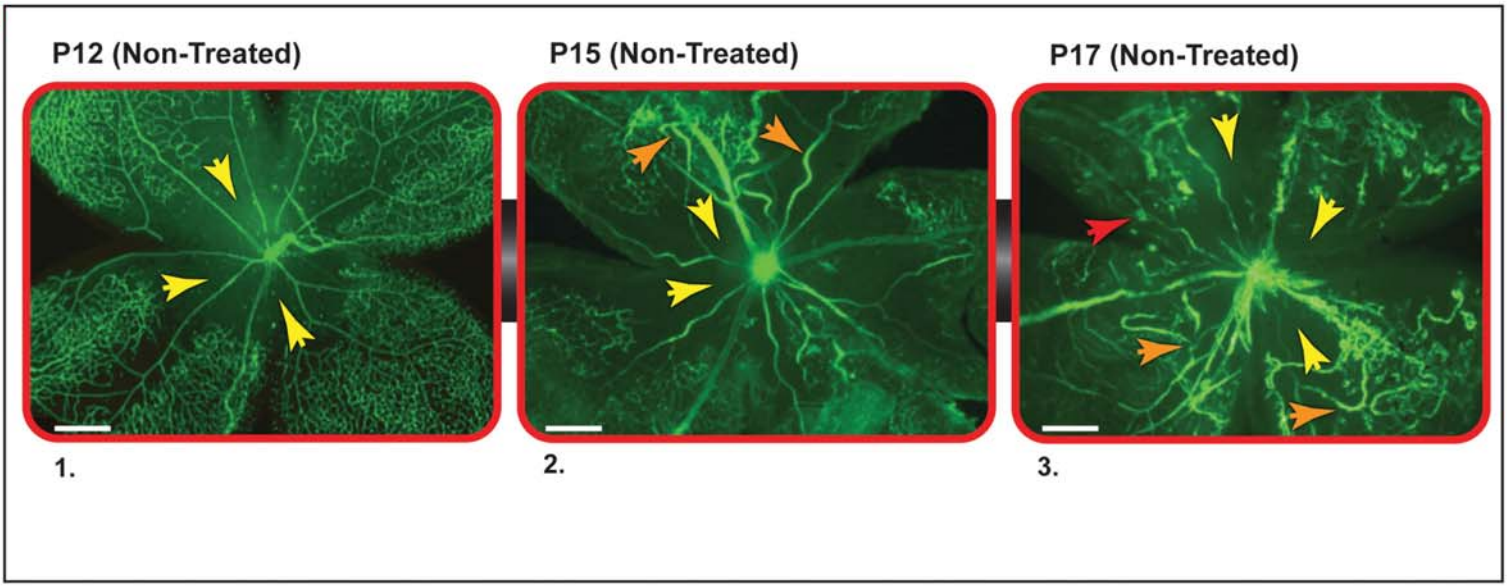

Molecular Pharmacology Fast Forward. Published on December 14, 2009 as DOI: 10.1124/mol.109.061366
This article has not been copyedited and formatted. The final version may differ from this version.

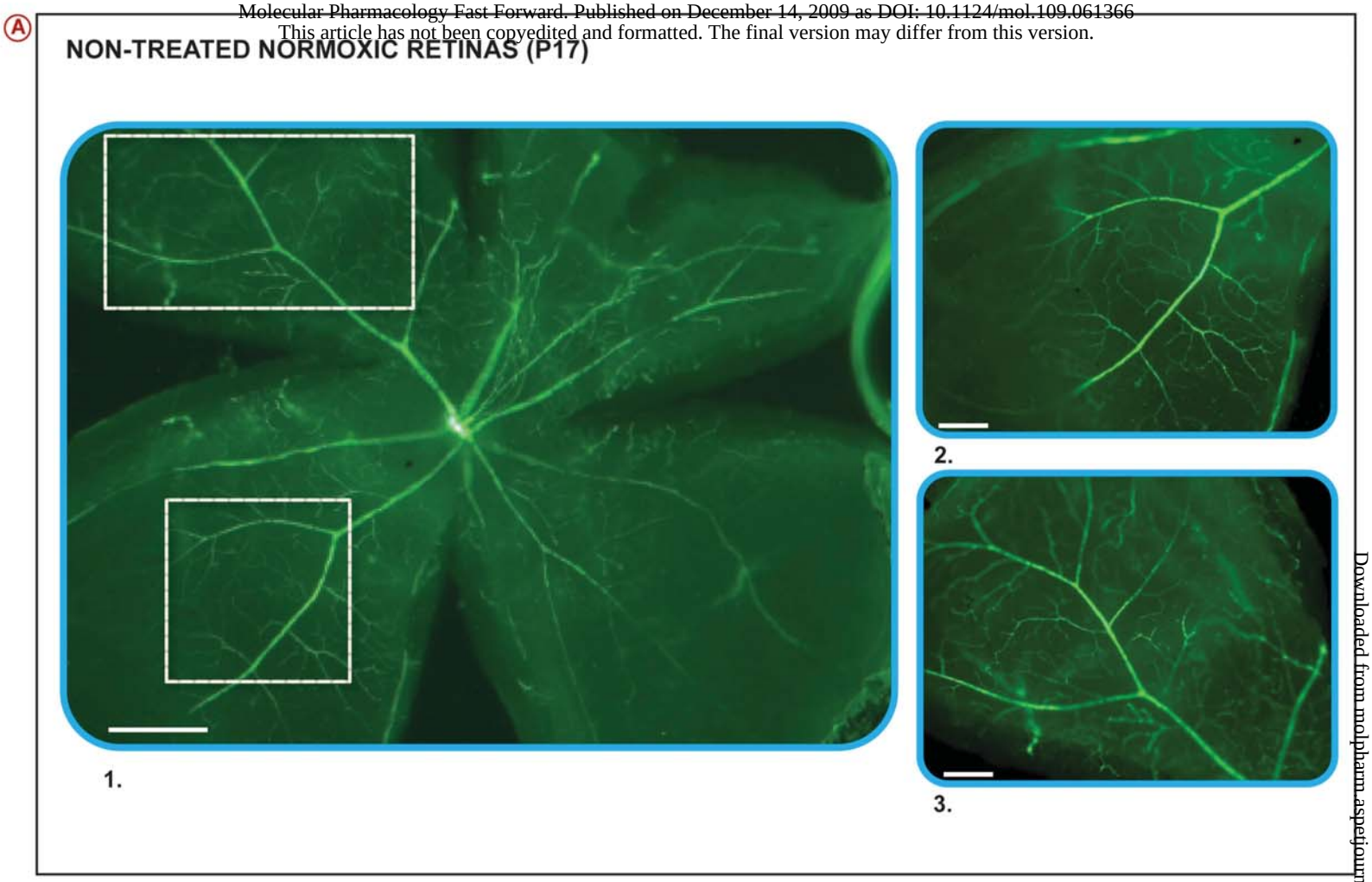

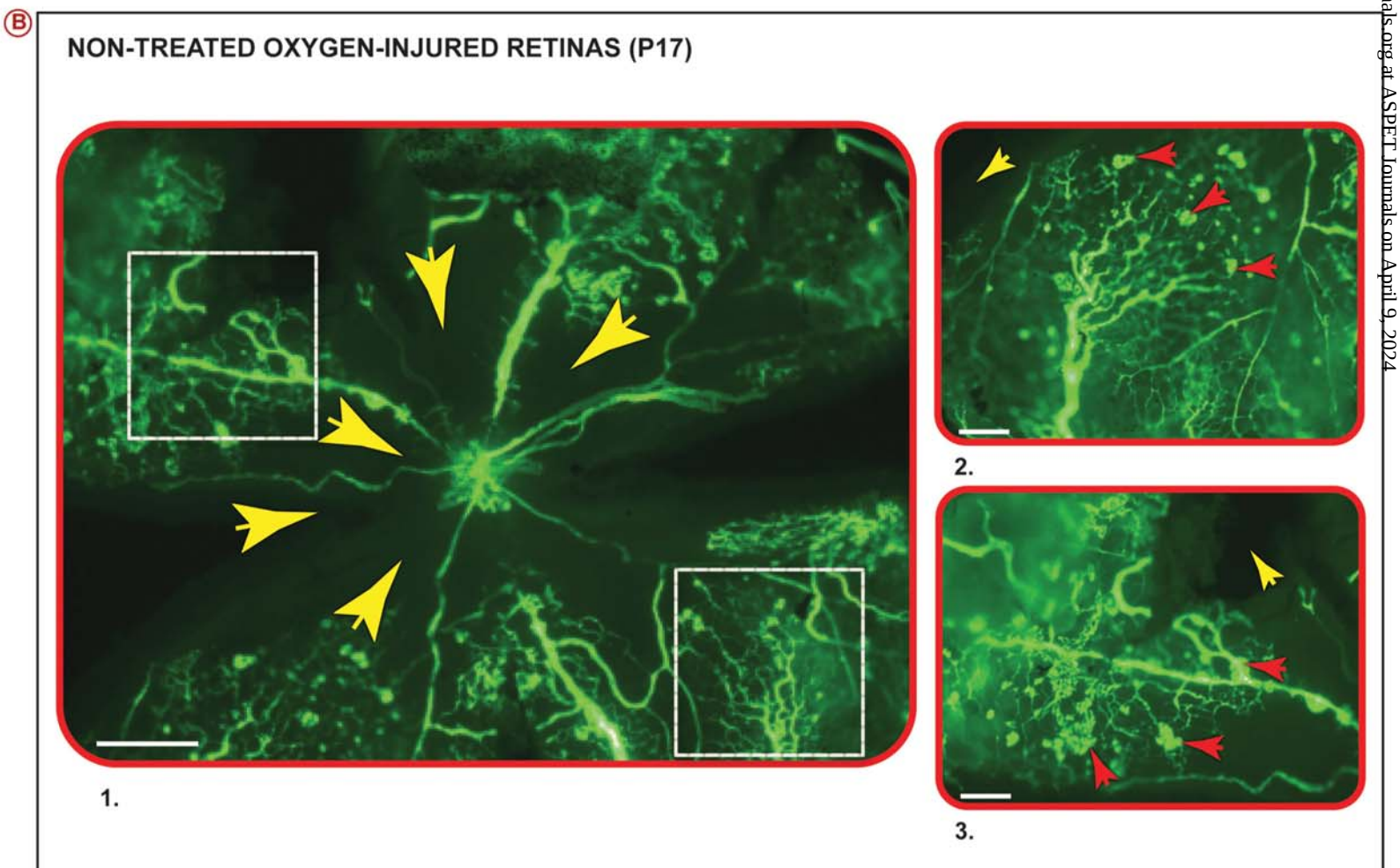

Figure 2 (cont'd overleaf)

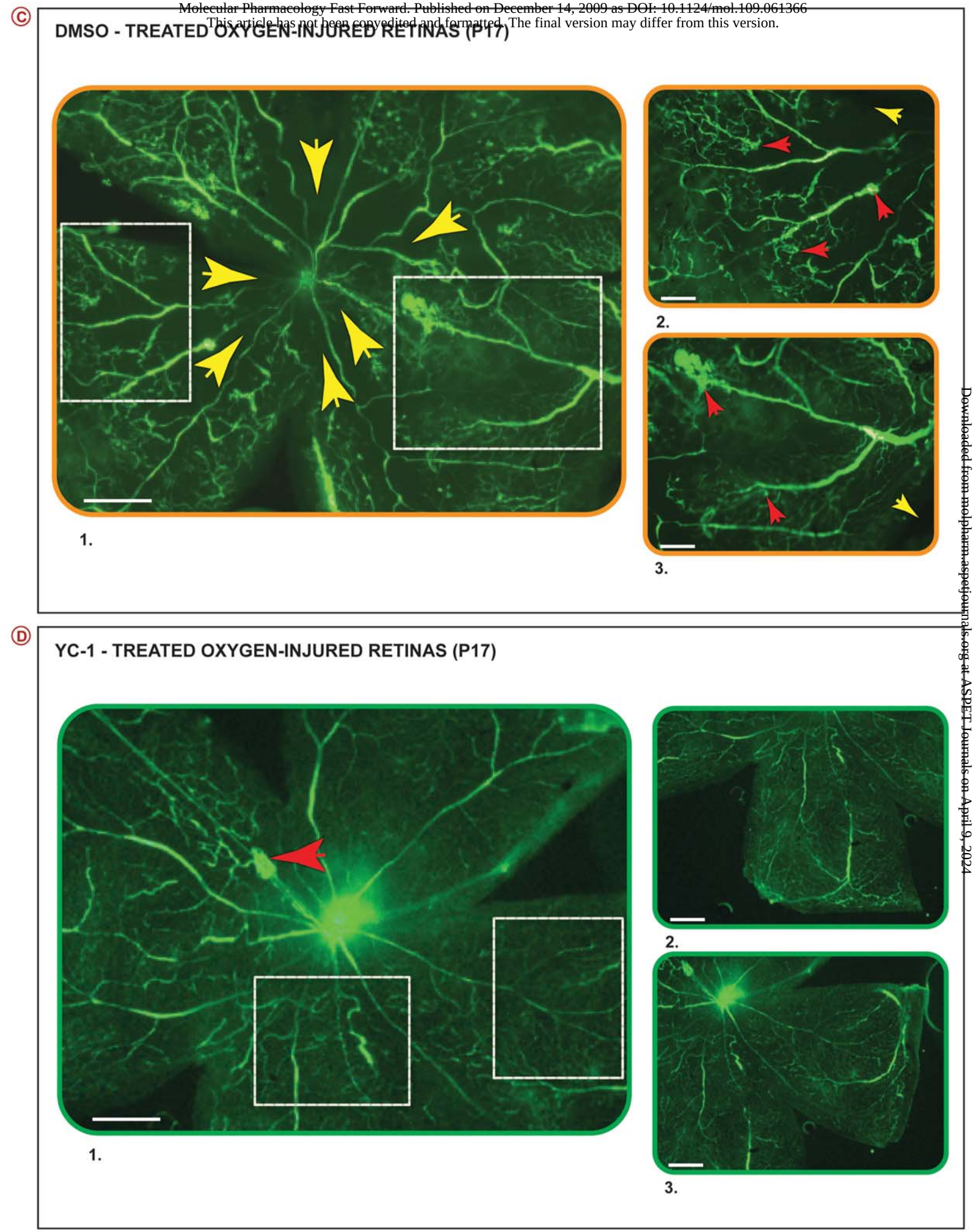

Figure 2 (cont'd)

Molecular Pharmacology Fast Forward. Published on December 14, 2009 as DOI: 10.1124/mol.109.061366
This article has not been copyedited and formatted. The final version may differ from this version.

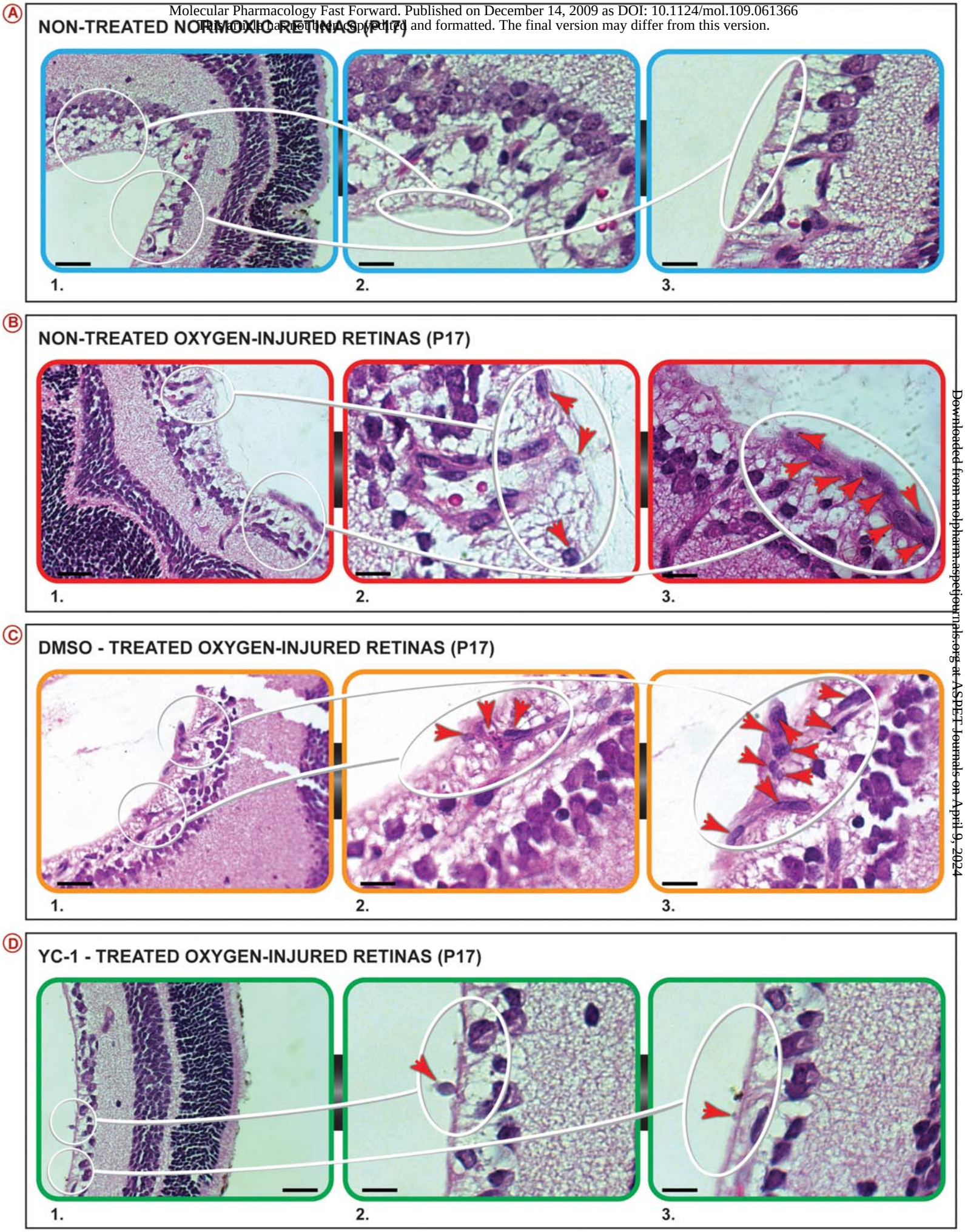

Figure 3

Molecular Pharmacology Fast Forward. Published on December 14, 2009 as DOI: 10.1124/mol.109.061366
This article has not been copyedited and formatted. The final version may differ from this version.

Ⓐ

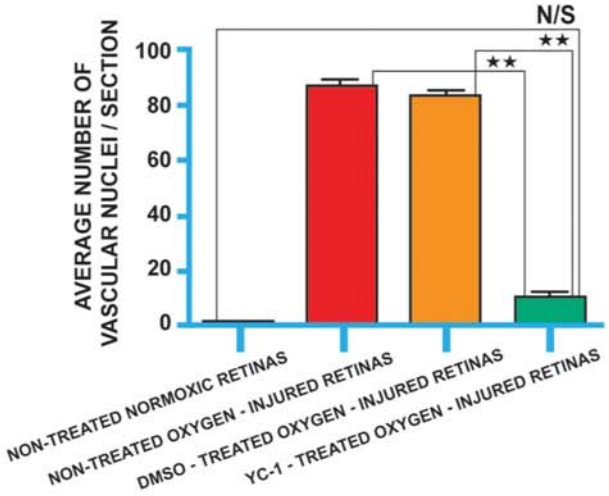

Ⓑ

Retinopathy Scoring System

	0	1	2	3	4
Central Avascular Area	none or < 50% of inner zone	< 25% of inner and middle zone	25-50% of inner and middle zone	> 50% of inner and middle zone	–
Blood Vessel Tufts	none	few, scattered in < 3 clock hours	in 3–5 clock hours	in 6–8 clock hours	9–12 clock hours
Presumed Extra-Retinal NV	none	mild in < 3 clock hours	moderate in 3–6 clock hours	severe in > 6 clock hours	–
Blood Vessel Tortuosity	none	mild in < 1/3 of vessels	moderate in < 1/3-2/3 of vessels	severe in > 2/3 of vessels	–

Ⓒ

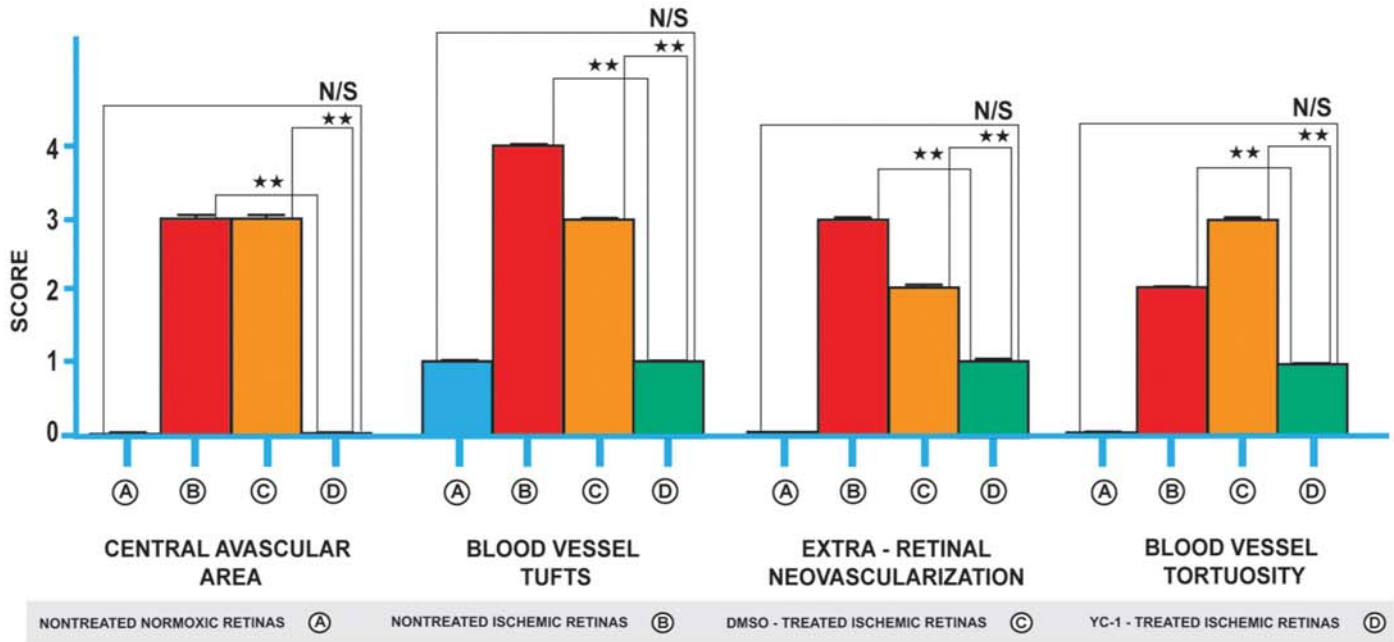

Figure 4

Molecular Pharmacology Fast Forward. Published on December 14, 2009 as DOI: 10.1124/mol.109.061366
This article has not been copyedited and formatted. The final version may differ from this version.

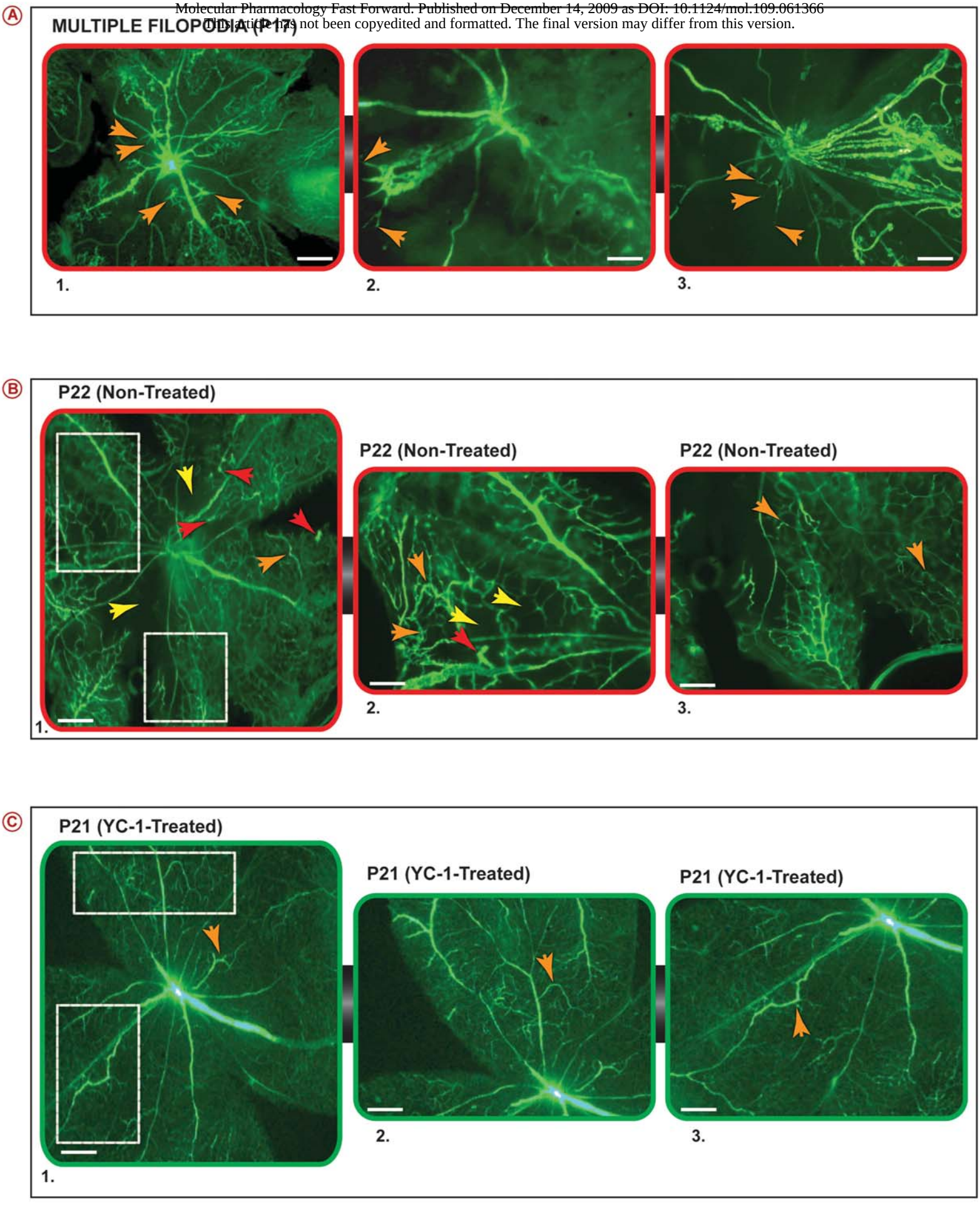

Molecular Pharmacology Fast Forward. Published on December 14, 2009 as DOI: 10.1124/mol.109.061366
This article has not been copyedited and formatted. The final version may differ from this version.

Figure 6

Molecular Pharmacology Fast Forward. Published on December 14, 2009 as DOI: 10.1124/mol.109.061366
This article has not been copyedited and formatted. The final version may differ from this version.

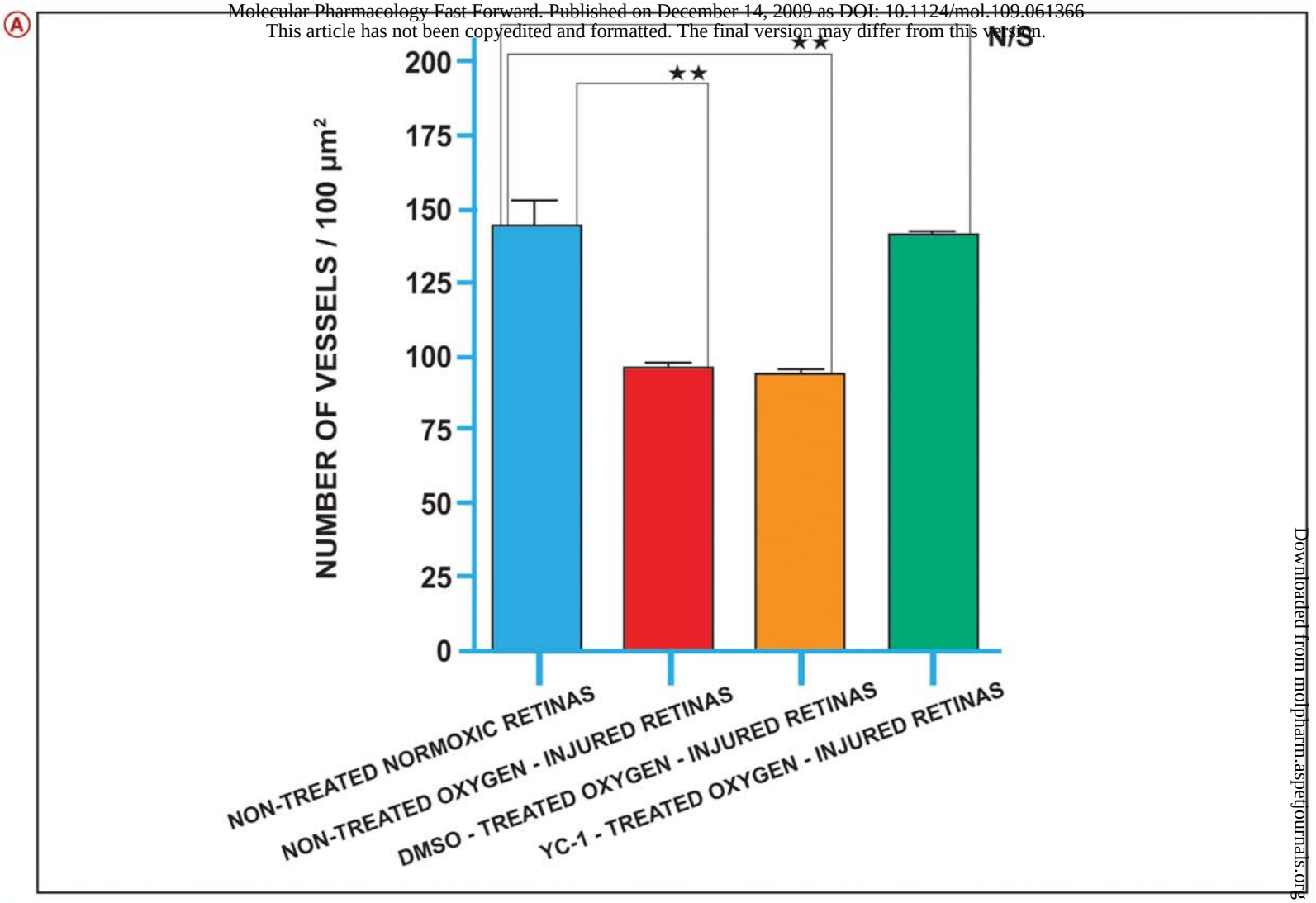

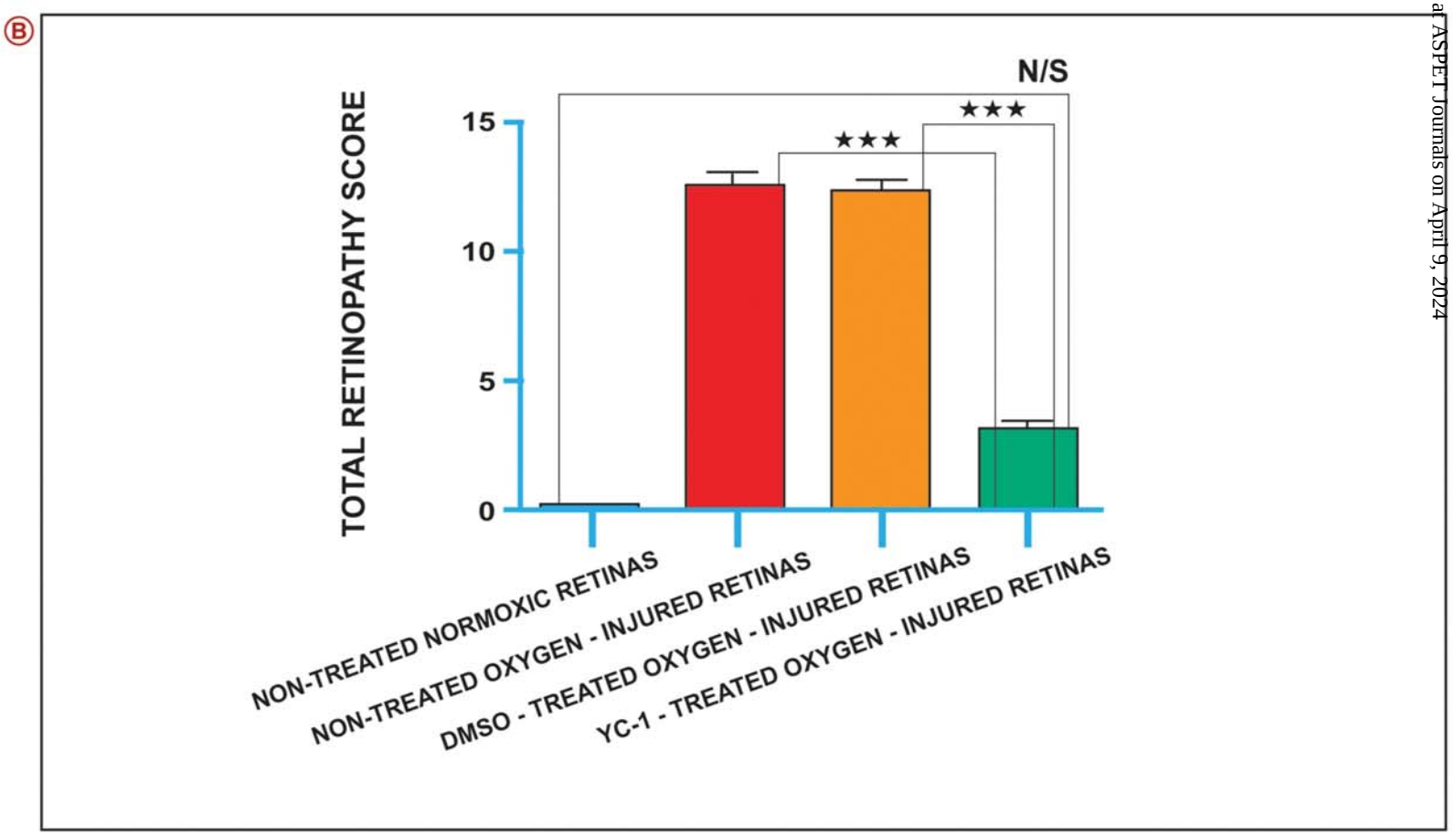

Molecular Pharmacology Fast Forward. Published on December 14, 2009 as DOI: 10.1124/mol.109.061366
This article has not been copyedited and formatted. The final version may differ from this version.

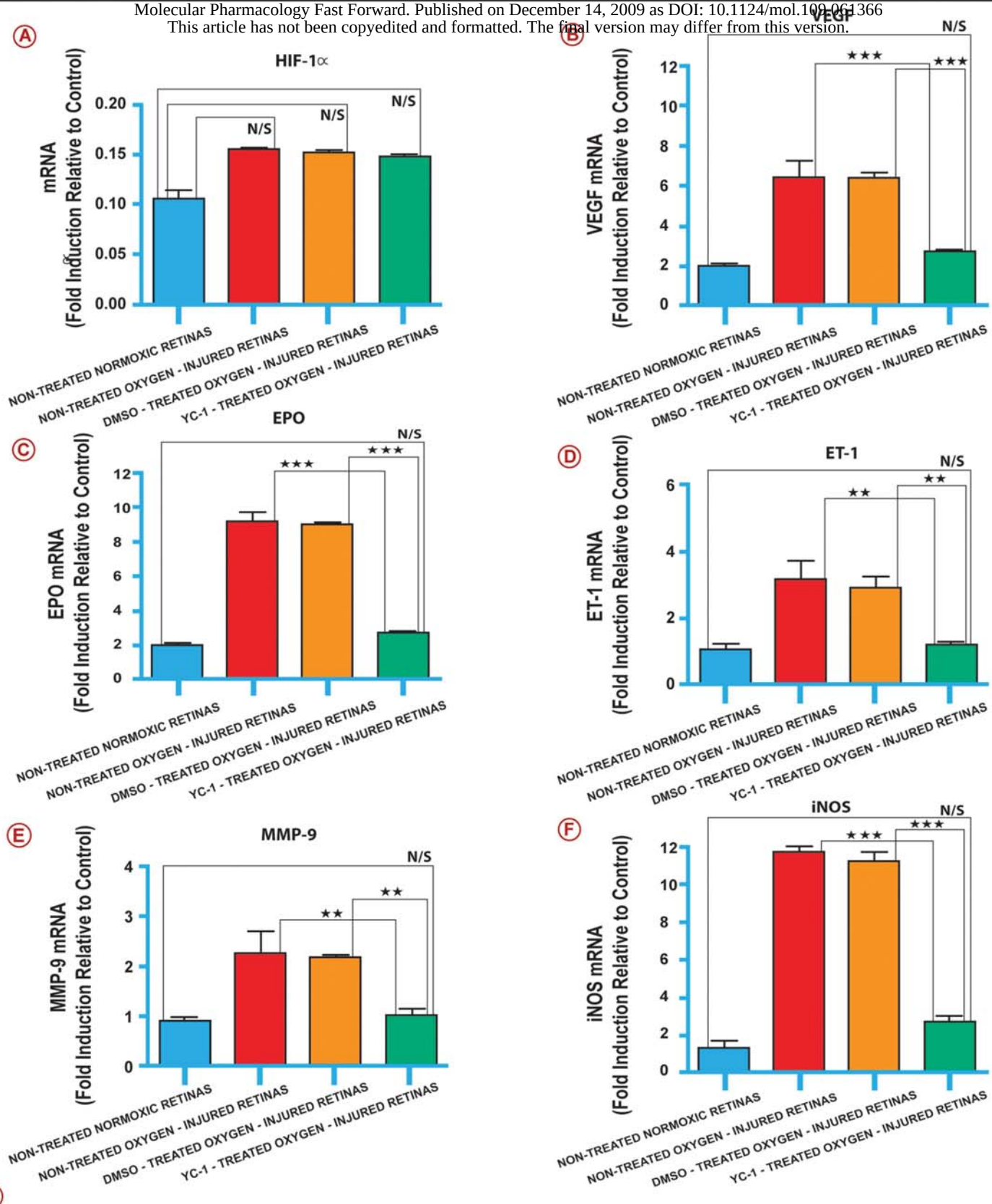

G

Sequence of molecular beacons and the primers used for the quantitative real-time PCR analysis

Sequence Definition	NAME	5' label	Beacon Sequence	3' label	Forward Prime	Reverse Primer
Beta Actin	RBA	FAM	CGCGATCACACAGAGTACTTGCGCTCAGGAGGAGGATCGCG	DABCYL	GCTGACAGGATGCAGAAGG	TGGAAGGTGGACAGTGAGG
HIF-1 ∝	RHIF1A	FAM	CGCGATCCCAAGCACGTCATAGGCGGTTGATCGCG	DABCYL	GTGTATGATACCAGCAGTAACC	ATGTTTGATGGATGAGGAATGG
VEGF	RVEGF	FAM	CGCGATCCTCATCTCTCCTATGTGCTGGCTTTGATCGCG	DABCYL	ACGTCACTATGCAGATCATG	TGTTCTATCTTTCTTTGGTCTG
EPO	REPO	FAM	CGCGATCATGGCTTCTGAGAGCAGAGACAGGCGATCGCG	DABCYL	GAATGAAGGTGGAAGAACAGG	GTGGCTGGGAGGAATTGG
ET-1	RENDO	FAM	CGCGATCAGATGATGTCCAGGTGGCAGAAGTAGAGATCGCG	DABCYL	CTCCTGCTCCTCCTTGATG	GGCTTCCTAGTCCATACGG
MMP- 9	RMMP9	FAM	CGCGATCGCTGGATGCCTTTTATGTCGTCTTCATGATCGCG	DABCYL	ATGTACCCCATGTATCACTACC	CCTTGGGTCAGGTTTAGAGC
iNOS	RiNOS	FAM	CCGACGCGTGGAAGCCCAAGTACGCGTCG	DABCYL	TGAGAGAGCAGAGGAAAATGAAC	CAAGGAATTATACACGGAAGG

Molecular Pharmacology Fast Forward. Published on December 14, 2009 as DOI: 10.1124/mol.109.061366
This article has not been copyedited and formatted. The final version may differ from this version.

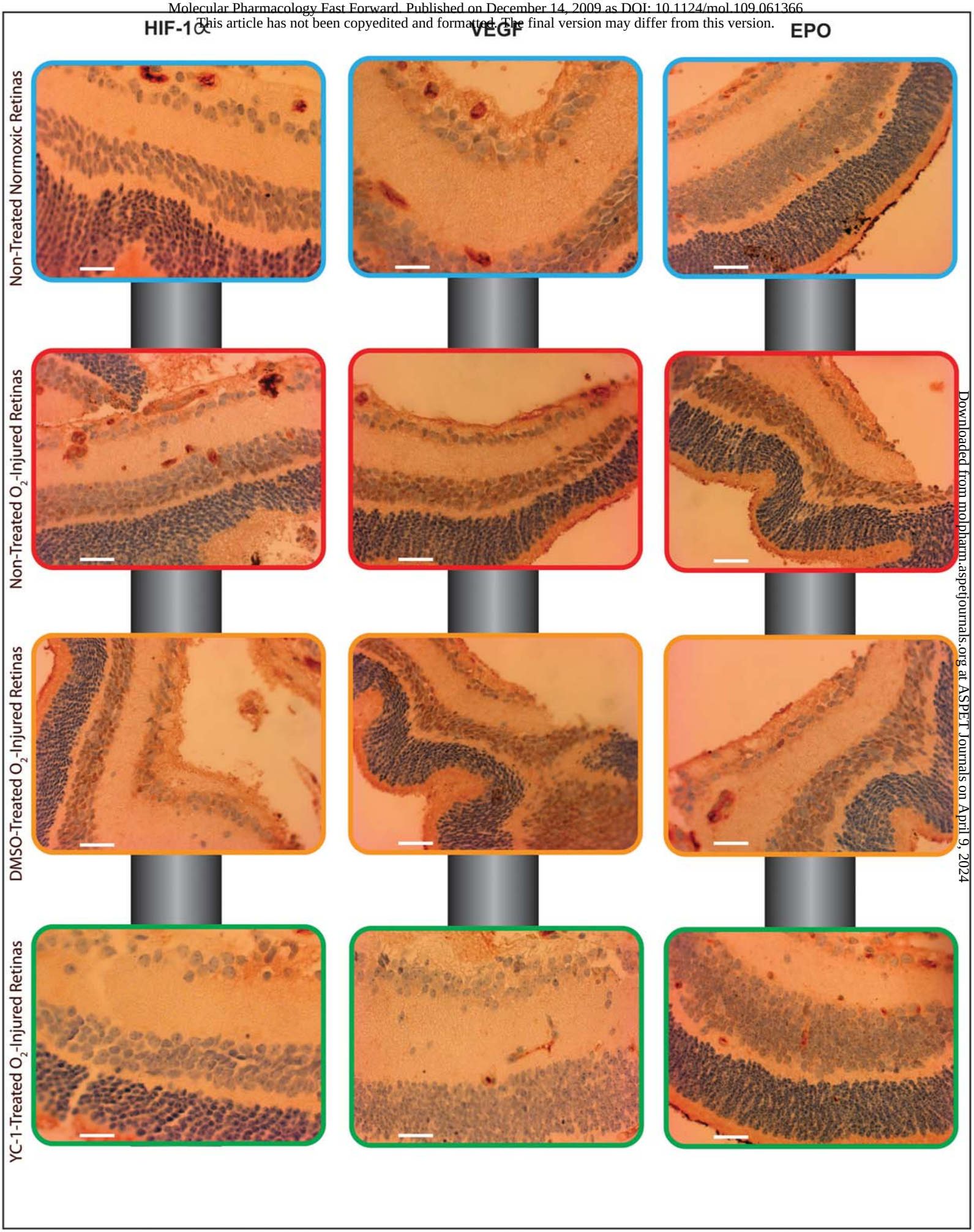

Figure 9 (cont'd overleaf)

Molecular Pharmacology Fast Forward. Published on December 14, 2009 as DOI: 10.1124/mol.109.061366
This article has not been copyedited and formatted. The final version may differ from this version.

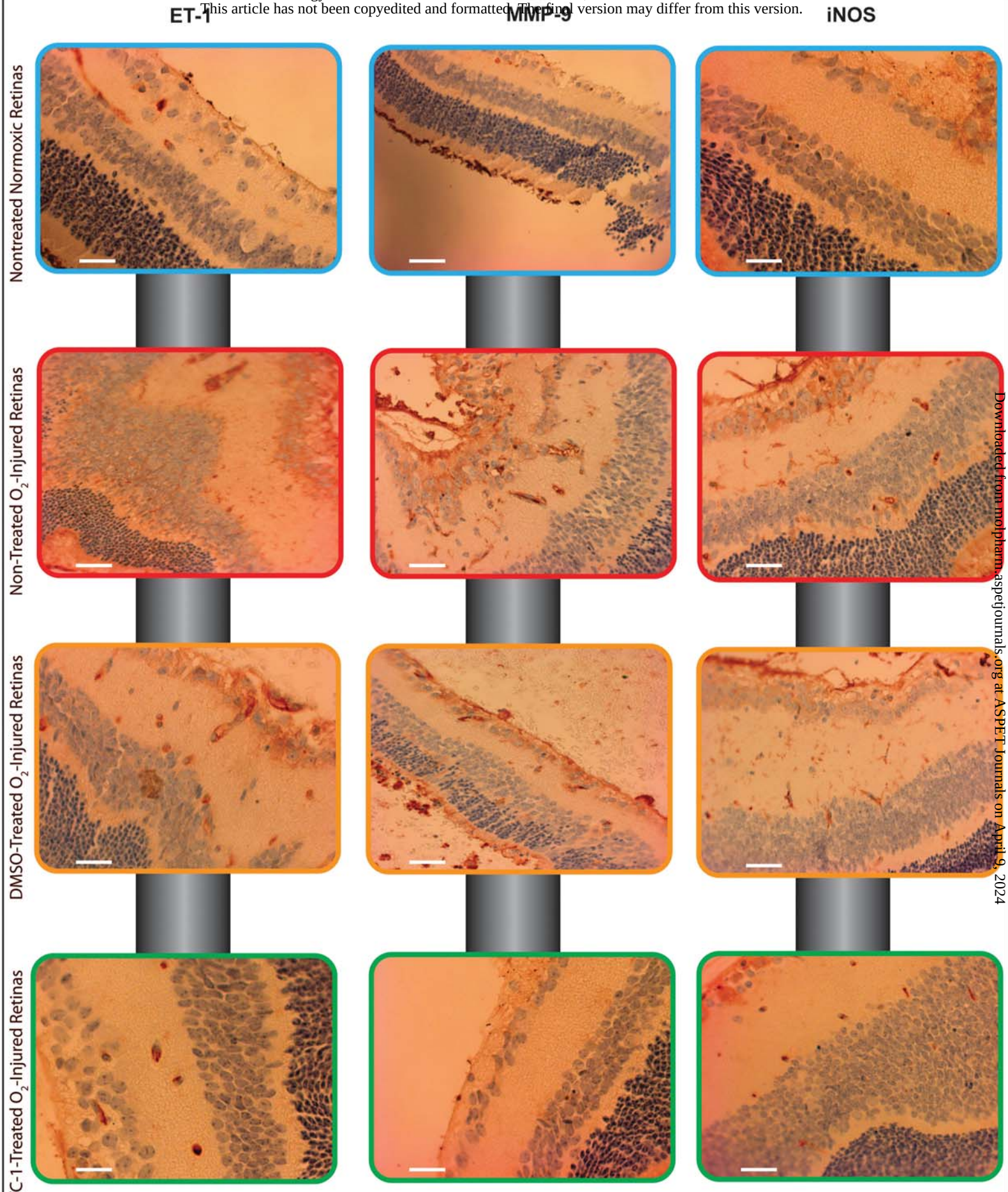

Figure 9 (cont'd)

Molecular Pharmacology Fast Forward. Published on December 14, 2009 as DOI: 10.1124/mol.109.061366
This article has not been copyedited and formatted. The final version may differ from this version.

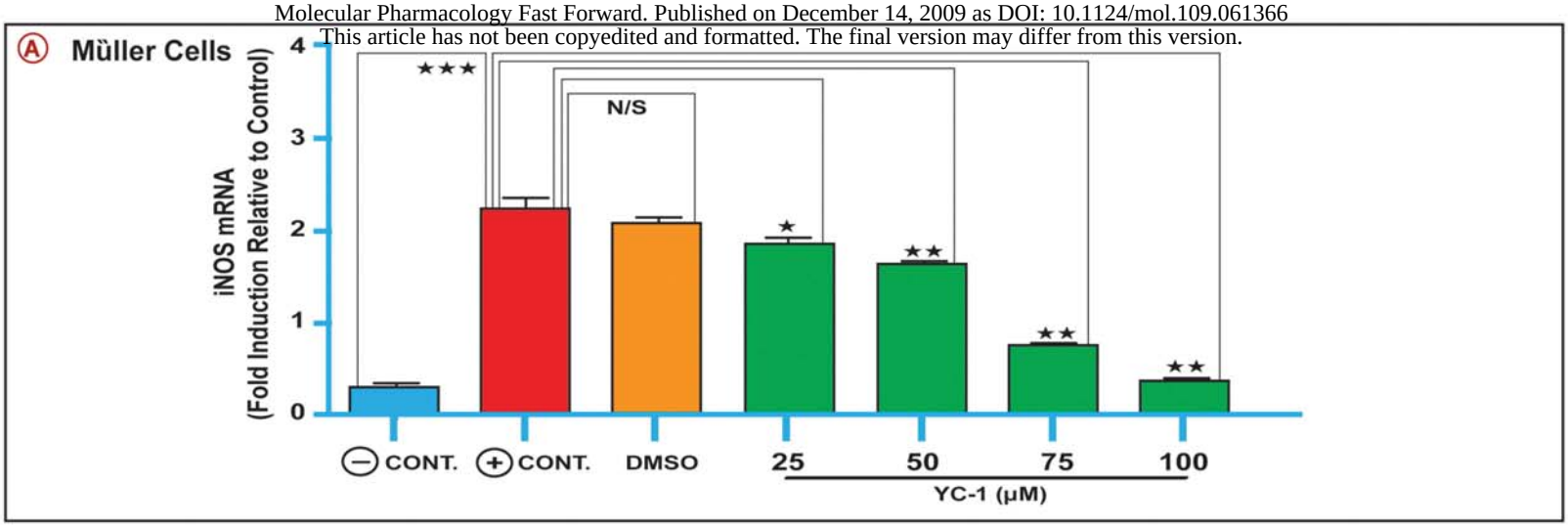

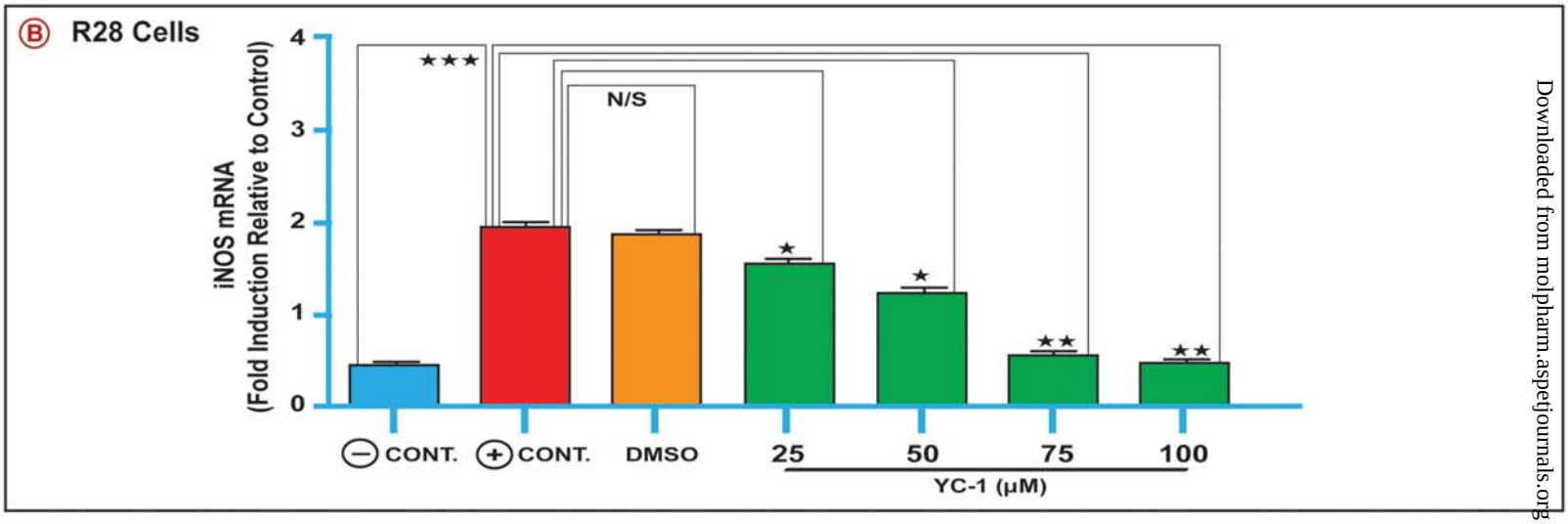

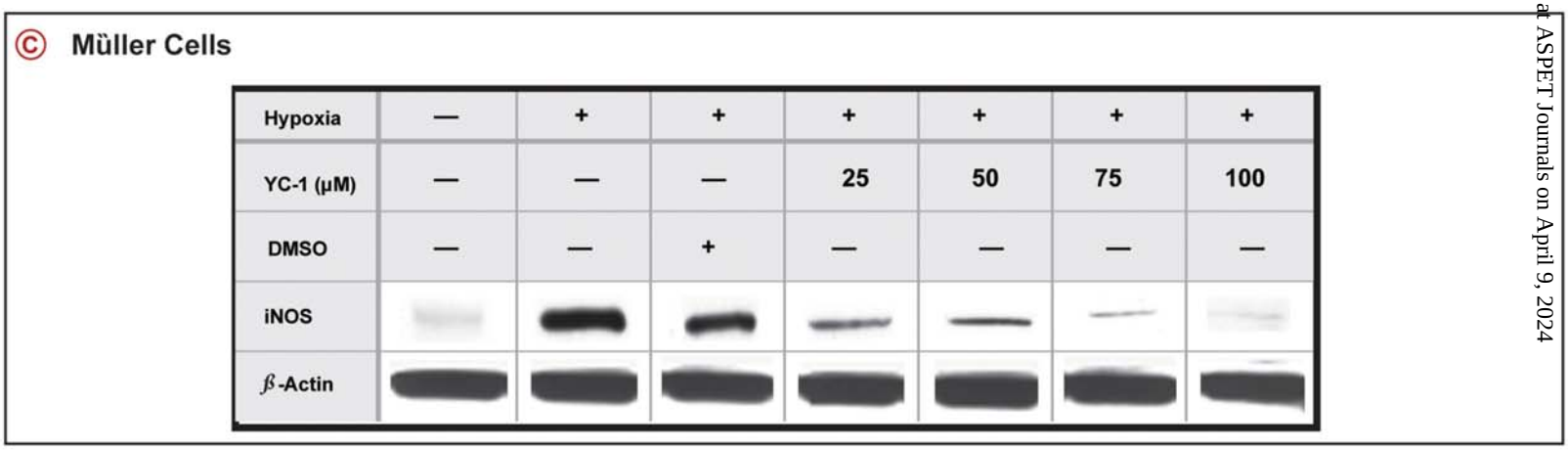

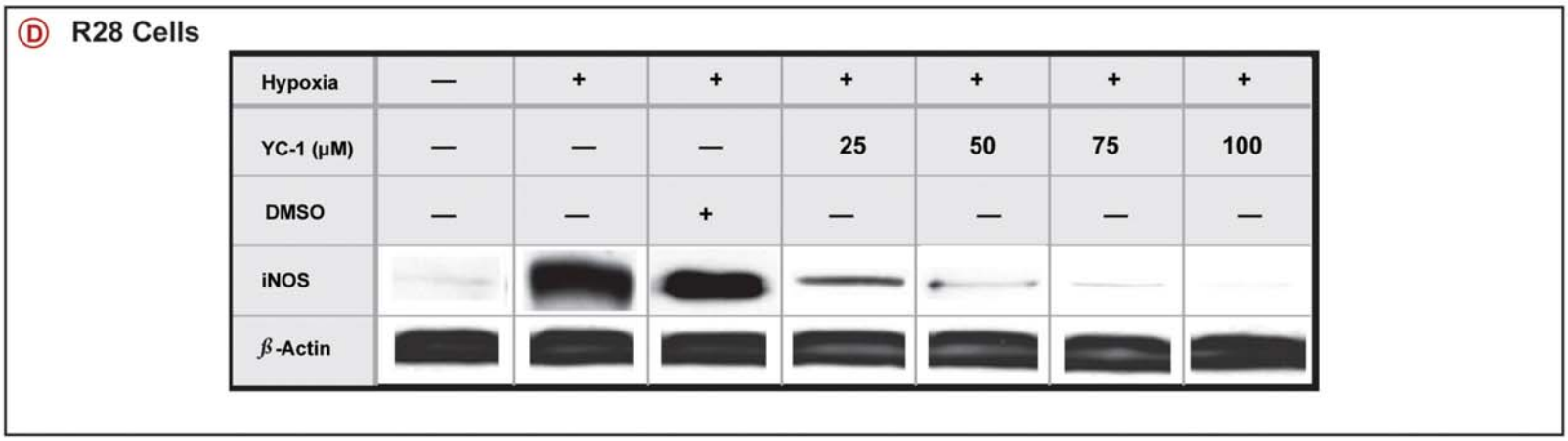

Molecular Pharmacology Fast Forward. Published on December 14, 2009 as DOI: 10.1124/mol.109.061366
This article has not been copyedited and formatted. The final version may differ from this version.